DOE Document Number
C00 ~~NYO~~ - 3425 - 16

MEASUREMENT OF AIRBORNE RADIOACTIVITY AND ITS METEOROLOGICAL APPLICATION

Part VII

by

R. Reiter, H.-J. Kanter, R. Sládkovič, W. Carnuth

and

K. Pötzl

Institut für Atmosphärische Umweltforschung
der Fraunhofer-Gesellschaft
zur Förderung der angewandten Forschung

D-8100 Garmisch-Partenkirchen
W-Germany

Annual Report
1st August 1975 through 31st July 1976

Prepared for the U.S. Department of Energy
Division of Biomedical and Environmental Research

EY-76-C-02-3425-A001

June 1978

DISCLAIMER

DOE Document Number
Coo ~~NYO-~~ 3425-16

MEASUREMENT OF AIRBORNE RADIOACTIVITY AND ITS METEOROLOGICAL APPLICATION

Part VII

by

R. Reiter, H.-J. Kanter, R. Sládkovič, W. Carnuth

and

K. Pötzl

Institut für Atmosphärische Umweltforschung
der Fraunhofer-Gesellschaft
zur Förderung der angewandten Forschung

D-8100 Garmisch-Partenkirchen
W-Germany

Annual Report
1st August 1975 through 31st July 1976

Prepared for the U.S. Department of Energy
Division of Biomedical and Environmental Research

EY-76-C-02-3425-A001

June 1978

Table of contents

page

page

I. OBJECTIVES AND ACTIVITIES OF REPORTING PERIOD

1. General

The basic objectives have been described in detail in the previous reports (Report I - VI). The aspects presently under study are following below:

a) Identification of stratospheric intrusions by observation of the time variation in the concentration of cosmogenic radionuclides. For this purpose daily aerosol sampling at the station Zugspitze with subsequent chemical processing for the determination of the activity of the radionuclides Be7, P32, P33, and S35, and of the fallout.

b) Calculation of the isentropic trajectories for the influx to the Zugspitze for selected long-term periods.

c) Derivation of a climatology of the stratospheric-tropospheric exchange from many years' series of data.

d) Testing of a method for the forecast of stratospheric intrusions.

e) Monitoring of stratospheric aerosol layers.

f) Preparation of a well-balanced program for the determination of the tropospheric ozone at different altitudes.

g) Continuation of the study of the influence of solar events on the stratospheric-tropospheric exchange.

2. Characterization of Particulars, Objectives, and Activities During the Reporting Period

The main characteristics of the activities during the reporting period are set forth in the following.

2.1. Aerosol Sampling and Radiochemical Analysis

Aerosol sampling at Zugspitze peak, chemical processing of the filters and the measurement of the concentration of the radionuclides Be7, P32, P33, and S35 have been continued. Great care has been bestowed on obtaining homogeneous measuring sequences to secure sufficient data for the planned future climatological evaluation of the stratospheric-tropospheric exchange.

2.2. Ozone Measuring Program

The measurement of the ozone concentration at the Zugspitze was continued. At the same time a program for the measurement of the tropospheric ozone has been evolved permitting an establishment of a balance of the tropospheric ozone. For this purpose it is planned to conduct synchronous measurements of ozone concentration at the stations Garmisch 700 m a.s.l.), Wank (1800 m a.s.l.), and Zugspitze (3000 m a.s.l.). Realization of this plan is in progress.

2.3. Forecasting of Stratospheric Intrusions

The forecasting method for a prognosis of stratospheric intrusions, described in the previous report, has been concluded and a quality control was elaborated. The method has been checked again in a long-term test. The result proved very satisfactory.

2.4. Determination of Fallout

The GeLi-Gamma-Spectrometer set forth in the preceding Annual Report has been employed for an analysis of the fallout composition. In doing so, fresh fallout from a Chinese nuclear weapon test could be identified.

2.5. Stratospheric Aerosol

The existing lidar system has been further developed. After appropriate improvements and extensions monitoring of stratospheric aerosol layers can now begin. First preliminary tests have led to promising results.

2.6. Solar-Terrestrial Relationships

The results of the study into the impact of solar events on the stratospheric-tropospheric exchange, comprehensively represented in the previous report, could be rounded off by an harmonic analysis of the Be7 concentration. The study was aimed at elucidating possible periodicities and at comparing these with the frequency of solar rotation.

II. GENERAL METHODS EMPLOYED

The methods described in previous reports have been retained. The routine processing of aerosol samples as well as the sampling proper could be conducted without interruption.

Much effort has been spent on the improvement of the lidar system with the objective to allow continuous monitoring of stratospheric aerosol layers.

At the end of February the measurement of ozone at the Zugspitze had temporarily to be interrupted for technical reasons. To ensure continuous measurements radical improvements at the instruments turned out necessary. In order to avoid invalidation of measuring data by local pollution, a new pipe for the air to be measured had to be installed. Measurements will be resumed as soon as possible. Preparations for the measurement at the stations Wank and Garmisch are underway.

III. PRACTICAL EXECUTION OF LABORATORY PROCEDURES

1. Sampling, Chemical Analysis, Physical Methods

The method for the measurement of the concentration of the radionuclides Be7, P32, P33, S35 plus fallout has been retained. No problems were encountered.

2. Description of the Lidar System for the Measurement of Stratospheric Aerosol Layers and of the Evaluation Technique

The lidar system described below has been conceived as double-frequency lidar and serves for the measurement of concentration and size distribution of the tropospheric aerosol. In additon, the system can be used for the monitoring of stratospheric aerosol layers. In the following only those parts of the system are described which are necessary solely for measurements in the stratosphere. Special mention will be made of parts which serve for both tropospheric and stratospheric measurements or which are connected to each other by the instrument control.

In the first section a general description of the system can be found, in the second section improvements are described which have recently been made to put the system into a condition suitable for a systematic study of stratospheric aerosol layers. Following is now a complete description of the stationary lidar system.

2.1. The Lidar System

2.1.1. Laser Transmitter

The block scheme Fig. 1 shows the layout of the lidar system with data acquisition electronics. The beam of the horizontally mounted, Q-switched ruby laser with 694 nm

wavelength, 2 Joules peak energy and 1 sec^{-1} maximum pulse repetition frequency hits a 45 degree dielectric mirror and is directed upwards. This mirror is mounted on a motor-operated carriage together with a KDP frequency doubler, a second dielectric mirror, and a blocking filter for the residual red light. By shifting the frequency doubler into the laser beam, a second transmitter wavelength (347 nm) is generated.

2.1.2. Receiver Unit

The backscattered laser light is collected by an astronomical quality 52 cm dia. Cassegrain telescope and fed through an image stop, an optical shutter, a filter wheel containing 3 nm bandwidth interference filters for the two transmitter wavelengths, a grey wedge, and a collimating quartz lens to the EMI 9816 photomultiplier tube (PMT) with S 20 cathode. This tube is mounted in a commercial cooling box with a double-walled heated quartz window. Coaxially above the secondary mirror of the telescope, the above-mentioned carriage for the deflecting mirrors and the frequency doubler is mounted.

Telescope, PMT assembly and carriage are contained in a barrel-shaped, waterproof housing closed on top by a tilted quartz glass plate, providing good transmission for the 347 nm transmitter wavelength, and carrying the horizontal exit window for the laser beam in its middle.

2.1.3. Fluorescence Suppression

The non-coherent fluorescent light emitted by the ruby in addition to the Q-switch pulse may be backscattered by close-range dust and interfere with faint return signals from higher altitudes. For this reason an electromechanical chopper is available which is synchronized with the

Q-switch and which blocks the laser beam path totally 136 microseconds after the laser firing, corresponding to 21 km altitude. Measurements with and without using this device showed the rejection of the fluorescent light to be absolutely necessary for getting reliable high-altitude signals.

2.1.4. Transmitter Energy Monitoring

The considerable scatter in output energy of the ruby laser even with well regulated flashlamp power requires monitoring the energy of each individual laser pulse in both frequencies. For this purpose, the light reflected back from the slightly tilted exit window of the receiver case is directed to a diffuse mirror consisting of a teflon plate which is polished to facilitate cleaning. From this mirror the diffusely reflected light, i.e. the light reflected under an angle not coinciding with the reflection angle of a plane mirror, is fed through a light pipe system to two photodiodes. The application of filters guarantees that each photodiode is sensitive only to one of the two transmitter wavelengths. The output pulses of both diodes, which are related to the laser beam intensity, are fed via only one cable to a 4 bit peak digitizer. Both diodes are calibrated by comparative measurements with a volume-absorbing calorimeter. This calorimeter itself contains a heating coil for calibration purposes. A precise rectangular pulse delivered by a special calibration unit is applied to this coil, which represents a measurable amount of energy. By this manner, an absolute calibration of the calorimeter is achieved which can be repeated as often as necessary. Simultaneous measurements with photodiode and calorimeter require the latter to be mounted above the laser beam exit window, i.e. in the open air above the receiver case. By this reason the very small energy readings induced by the frequency doubled laser

beam are often superposed by heavy fluctuations due to ambient radiation and wind, or by constant zero point offsets caused by internal temperature gradients within the calorimeter. Both deviations may exceed the measuring-signals by orders of magnitude. The fluctuations can greatly be reduced by shielding the calorimeter, but the constant dc offsets remain even if the calorimeter is well isolated. For this reason, and since only a normalization, not an absolute calibration of the transmitter is essentially necessary, we calibrated both photodiodes additionally by a layer diode transmitter. Its emitted light was attenuated by grey filters with known transmissivity.

The measurements resulted in following relative calibration curves, normalized to give unit incident intensities I for a peak digitizer reading of n = 10:

$$694 \text{ nm} : \quad I = .0439n + .56$$

This result indicates the 694 nm photodiode amplifier characteristic to have a zero point offset. This is in good agreement with earlier calorimeter measurements.

The absolute calibration of the photodiodes (which is, as mentioned above, not essentially necessary) only requires one constant factor k (λ) for both diodes to be evaluated:

$$E(\lambda) = I(\lambda) \cdot k(\lambda) \quad [\text{Joules}]$$

The calorimeter measurements give K (694 nm) = .89.

2.1.5. Data Acquisition

The signals delivered by the PMT are fairly smooth curves if their amplitudes are high enough. Weaker signals from higher altitudes show a spiky nature, increasing with decreasing amplitude, due to the beginning resolution into single photon peaks. Signals from very high altitudes,

finally, are still consisting of single photon peaks with varying frequency, but constant amplitude distribution. This circumstance is to be taken into account when designing the data recording. Two different ways of recording are possible in our system: Analog recording and photon counting, the latter being used for monitoring of the stratospheric aerosol.

2.1.5.1. Photon Counting (see Fig. 1)

As mentioned above, PMT signals with decreasing amplitude are resolved more and more into single photon peaks. Signals of this kind may be processed in different ways. One method is the analog integration over a certain period of time or distance. Another one is the photon counting method, which offers the advantage of an increased signal-to-noise ratio, as by means of pulse-height discrimination any low-amplitude noise from the PMT or the electronics may be rejected. In our system a ten-channel multiplex photon counter is available with presettable delay and gating time. This means the first counting channel is "opened" at the preset time after the laser shot, which is indicated by a trigger signal from the photodiode ADC. After the preset gating time has elapsed, the first channel is "closed", the second one "opened" and so on until the tenth channel is closed after ten times the gating time. An eleventh channel serves as reference channel and is opened 5 millisec. after the laser shot. It counts the photon pulses from the PMT dark current and from any residual skylight background. Parallel to the gating of the eleven channels a pulse is applied to a special circuit to gate the photomultiplier tube. For this purpose the dynode chain has been changed in such a way that in the quiescent state the voltage between dynodes 1 and 2 and between dynodes 6 and 7 is reversed, resulting in a nearly

zero overall gain of the tube. By special high-voltage switching transistors, the voltages of dynodes 1 and 6 are switched to their "normal" values within the dynode chain, allowing the PMT to get its usual high current gain, as long as the ten counting channels and the reference channel are open. This device prevents overloading of the tube by strong close-range signals, and is useful also for analog recordings as mentioned above.

The transfer of the gating pulse from the photon counter to the dynodes gives rise to problems due to high potential differences which must be bridged. In our case high frequency transformers are used, providing sufficient bandwidth for undistorted transfer of pulses with small risetime. The length of the pulses to be transferred is limited, however, in our case to about 20 microsec., corresponding to a maximum total height interval of 3 km. This is a drawback in some cases. For example, it is desirable to start stratospheric measurements with low-resolution summary backscatter profiles with a moderate number of shots. For this reason a transformer-optical coupler combination has been developed which allows transferring pulses up to more than 200 microseconds in length without any sacrifice in bandwidth.

As mentioned above, the range gating prevents extremely high currents near the cathode of the PMT arising from the strong close-range backscatter signal, which otherwise could give rise to increased background noise immediately after the short-range signal peak. Nevertheless, our first measured profiles did show a superposed slowly decreasing background. This background was only partly caused by ruby fluorescence, in contrary to our first opinion, and must have its origin within the PMT itself. This was the reason for the installation of the double gating (in the first version only dynode No. 6 has been gated). The double gating decreases the residual closed-

gate signal by another four orders of magnitude, but unfortunately it doesn't affect the background very much. Experiments showed, however, that the background may be eliminated by reducing the PMT high voltage and by careful alignment of the input discriminator threshold as well as of the grey wedge. With 1850 Volts applied to the PMT, 9 Millivolts threshold and the grey wedge set to 6% transmissivity (or less for altitudes smaller than 20 km) we get reliable profiles up to 30 - 40 km. Examples of backscatter profiles are shown in part III.2.5.

2.1.6. Data Processing

The stored data from Biomation recorder and photon counter had to be output on punch tape after each laser shot for off-line processing and evaluation. This involved many drawbacks.

For the reasons just mentioned the desire for an on-line computer for real-time data processing arised. Since May 1976, a new Intertechnique Multi-4 minicomputer is available, with 8-bit, 16 k core memory, a high speed optical punch tape reader and a Tektronix 4006-1 graphic display terminal, allowing alphanumeric and graphic mode operation. A new interface has been developed allowing data transfer from photon counter & photodiode peak digitizer to the computer (or directly to the tape punch as before if desired). The interface is connected with the computer via an one-channel input-output interface. Eight parallel data lines are available plus three logic control lines. The first one is called "end of conversion" (EOC). It is set to logical high by the data record device (photon counter) immediately after a signal record has been finished. This is recognized by the computer (under program control), which then gives a command signal to the interface via the second control line. The interface (plus

photon counter) again answers with a flag signal via the third control line, which means the first data byte is ready for output. The computer program inputs this data byte, gives the next command signal, and so on, until all data bytes are transferred. This is signaled from the interface by setting the EOC line low.

A program has been developed for transferring the data as just described, performing the first steps of return signal evaluation for both analog and photon counting signals, and displaying the calculated backscatter profiles on the terminal screen. It will now be briefly described with the aid of the flow chart Fig. 1a, b.

As the computer cannot itself initiate the data transfer from the recording devices (this will be possible with the new interface described later) the program is started entering a waiting loop for EOC. The EOC is set high immediately after the data acquisition device has been triggered by a laser shot and the signal has been recorded. The Biomation recorder is to be set to the "automatic digital output" state by pressing a button. The EOC is set low if, depending on the position of a three-way switch at the interface, all data from the photon counter plus peak digitizer, Biomation recorder, or both, are transferred. Since we need the data from the photodiode for both types of signal recording, the position "Biomation alone" is never used.

As the "EOC high" is recognized, the program gives a command signal to the interface. If no command occurs 10m sec after the EOC is set high, (e.g. if the program has not been started), the interface automatically transfers the data to the punch tape. If the command is received in time by the interface, the flag signal is transferred to the computer as described above and the program inputs the data byte to the accumulator register. It then branches according to the type

of data recording being utilized (analog recording or photon counting). This is accomplished using one of four console sense switches available with the computer, which position may be "questioned" per program. In the case of photon counting, the data are output in double BCD code (photon count number digit plus channel number), and the data bytes stored in a special part of the memory. In the case of analog recording another decision is necessary in the program whether a backscatter signal or the constant sky background is to be measured. A second sense switch is used for this purpose. In each case the contents of the accumulator (Biomation data are delivered in binary format) is added to the contents of the corresponding memory location in a signal or background buffer (which is zero prior to the first shot), specified by the index number.

The next program steps are incrementing the index number and checking the status of the EOC line. If it is still high, the next data word is input, otherwise the program branches again. In the case of photon counting the number of photons per channel are converted to ASCII numbers and displayed on the terminal screen, while the binary numbers are output on punch tape. Furthermore, for the calculation of averages and standard deviations the photon counts and their squares are summed up for each channel. The energy monitor values are also summed up. In the case of analog recording only the energy monitor sum is to be calculated.

The program then again enters the starting loop. This loop contains a check of the third sense switch. It is pressed if "end of series" occurs, i.e. if the current series of shots is to be finished. In this case for photon counting the sum of the energy monitor values and the range gate data (delay and gate length) are output on punch tape, and the energy-normalized and range-corrected backscatter

profile displayed on the terminal screen together with the statistical error bars. Looking at this display it may be decided whether additional measurement should be made or not.

The final evaluation of photon counting data is still done using our main computer with the precision incremental plotter.

2.2. Improvements at the Lidar System

2.2.1. Parts of the System which have not been changed

The following parts of the system have not essentially been changed in the meantime:

- the Q-switched ruby laser transmitter with 694 nm wavelength, 100 MW peak output power and 1 Hz maximum pulse repetition frequency
- the power supply for the laser and the Q-switch
- the fluorescence suppression
- the energy monitor with peak digitizer
- the fixed vertical Cassegrain receiving telescope with 52 cm diameter
- the gain switching amplifier
- the photon counter with range gating
- the preamplifier
- the on-line computer with graphic display terminal and punch tape output.

2.2.2. Improvements and Extensions of the Stationary System Since July 1976

During the recent past several improvements and extensions to the lidar system hardware have been performed. The major part of the innovations concerns the improvement of the data acquisition and the automation of the system operation, a smaller part the transmitter-receiver system.

For the sake of clearness not all control lines are included in Fig. 1; they are shown completely in Fig. 2 which will be described below. Following is now a detailed description of the innovations:

2.2.2.1 Special Photomultiplier for Photon Counting

The EMI photomultiplier tube is not specially designed for photon counting purposes. The quite low secondary emission factor at the dynodes (2 - 5, depending on the applied voltage) causes heavy statistical fluctuations of single photon peaks. The resulting broad pulse height distribution curve renders very difficult or impossible at all an exact discrimination between signal and noise pulses. So we found a slowly decreasing background superposed on the return signals, probably due to the strong close-range signal in spite of the range-gating of the tube, if the full sensitivity of the receiver, without any attenuation by the grey wedge, was used. This background could only be eliminated by reducing the received backscattered light by a factor of 10. Furthermore, the pulse frequency resolution of the EMI 9816 tube proved to be quite low, probably due to the high number of dynodes. For these reasons the acquisition of a complete backscatter profile from 6 to 30 km altitude required the application of a great number of different grey wedge settings in order to get suffi-

cient counting statistics on the one hand and avoid excessive pulse overlapping on the other.

For these reasons a RCA 8852 photomultiplier tube has been provided. This tube is equipped with a gallium phosphide coated first dynode, providing a secondary emission ratio of up to 50 at this dynode and consequently a greatly improved counting statistics. First measurements revealed the performance of this new tube to be surprisingly much better than the EMI tube. Together with a new, faster photon counter input comparator, the pulse frequency range was extended by a factor of no less than 10. Furthermore, even with full receiver sensitivity no superposed background at all is observed with the return signals. Consequently, the total number of laser shots required for the measurement of a complete backscatter profile with given accuracy is now considerably reduced.

Unfortunately, at least at the time of commission of the tube no version was available with sufficient sensitivity as well for 694 nm as for 347 nm wavelength. So for analog measurements conducted in both frequencies the EMI tube is still to be used and is to be replaced by the RCA tube for stratospheric measurements performed with 694 nm wavelength only. In order to facilitate the change of the tubes, the heavy and unhandy photomultiplier cooling box, which proved to be unnecessary, was replaced by two separate smaller conventional housings for each tube with separate sockets and voltage divider networks allowing the change of the tubes within less than one minute. An example of stratosperic measurements with the new tube is presented in part III.2.5. of this report.

2.2.2.2. Polarizer for Measurement of Signal Depolarization

With the initial single-frequency version of the system a

polarizer was available in front of the photodetector. The plane of polarization was changed by turning the whole detector housing. With the onset of the two-frequency operation the polarizer was removed temporarily because the polarization plane of the 347 nm laser beam is perpendicular to that of the 694 nm beam, and the change of the transmitter frequency would have required each time the time-consuming turning of the photomultiplier case by 90 degrees. However, as the measurement of the signal depolarization is desirable for several reasons, a motor-operated turnable mount for the polarizer was fixed to the receiver which may be controlled from inside either munual or by the computer (see below).

2.2.2.3. Automatic Temperature Control for the Laser

The laser is cooled by a closed water circuit which is recooled by tap water by means of a heat exchanger. The exact wavelength of the ruby laser depends somewhat on temperature. In order to avoid unintentional tuning of the laser to one of the near-by water vapor absorption lines, a magnetic valve operated by a contact thermometer was applied to the tap water line. This valve stops the tap water flow if the temperature of the secondary circuit water drops below a preset value.

2.2.2.4. Floppy Disc Memory

In addition to the 16 K core memory a floppy disc memory is now available with the on-line computer. It consists of two separate units with 300 k capacity each and avoids the necessity of intermediate punch tape output of averaged signals during a series of measurements. Instead of that, any number of single signals may be stored on one or more floppy discs and output on punch tape later after finish-

ing a complete series of measurements. This device is also very convenient for storage of programs.

2.2.2.5. Neutral Filter Wheel

Previously the receiver sensitivity attenuation was accomplished by a continuous neutral or grey wedge, remotely operated by a magslip. Because it proved to be difficult setting the wedge to a certain attenuation value with sufficient reproducibility, it has been replaced by a motor-operated filter wheel with 3 discrete neutral filters and one empty hole (zero-attenuation position).

2.2.2.6. Devices for Complete Automatic Operation of the System

The Biomation 8100 transient recorder for analog recording of the tropospheric aerosol is fully externally programmable. For utilization of this possibility a special computer interface has been available for more than a year. However, the external programming of the transient recorder only seemed quite unsatisfactory, and so it was decided to develop additional electronic circuits allowing a completely automatic, computer-controlled operation of the whole system. This should include the following single operations:

- programming of the transient recorder
- laser start
- change of transmitter wavelength
- change of interference filter
- change of neutral filter
- setting of the photomultiplier high voltage
- setting of range gate length and delay
- triggering of the data acquisition electronics for the measurement of the skylight background

- change of the polarizer position.

The control electronics which has been developed here at the Institute by our co-workers (see Fig. 2) will now be described in detail, including a modified data transfer from transient recorder and photon counter, guided by Fig. 2.

2.2.2.6.1. Input/Output Control Facilities of the Computer

For the exchange of data between computer and external devices two 32-bit input/output controllers are available. The input and output lines are divided into four groups or channels à 8 bit each, which are accessed by channel select function codes from the computer. During an output transfer, the 8-bit word from the computer is loaded into the input register of the selected channel, and an output data strobe pulse is issued to the device. During an input transfer, the 8 input lines from the selected channel are scanned by an input multiplexer and the resulting input word is supplied to the computer when "data in" occurs. Additionally an external interrupt line is available with each I/O controller.

2.2.2.6.2. Data Transfer

Previously, the data of both transient recorder and photon counter/peak digitizer had been transferred to the computer via interface No. 1. With the computer a single channel, 8-bit interface was used for this purpose which otherwise is destined for punch tape input and output. As with the I/O controllers sufficient input channels are available, one channel of controller No. 1 is now used for the data transfer from transient recorder and photon counter.

Data from photon counter/photodiode peak digitizer are still transferred via interface 1, the transient recorder data via the new interface 2. The usage of this interface offers several advantages. First, data recording may be done in the "off" mode of the recorder, allowing the examination of the data prior to the transfer to the computer. The data transfer is initiated by the computer by issuing a special instruction word to the recorder. Furthermore, for technical reasons the data transfer is much faster than with the former interface, which allows the transfer routine for one data word to be executed by the computer within less than 100 microseconds. Consequently, as the recorder memory made up of MOS shift registers needs refreshing between output words at read rates slower than 100 microseconds per word, the time required for the transfer of the total memory contents is reduced from 2.5 to about .2 seconds.

The usage of only one input channel for transferring both the transient recorder and photon counter data is made possible by tri-state outputs in both interfaces. An internal electronic switch operated by computer instruction, which is not included in Fig. 2, prevents simultaneous output from both interfaces.

2.2.2.6.3. External Range Gate Control

Previously the range gate length ("gate") and delay time ("delay") had been set manually by two 4-digit decimal switches each, in increments of .1684 microseconds. The 8 digits may now be set by the computer where for saving of output channels multiplex operation is used. The most significant 4 bits of the 8-bit word output from the computer are used as digit address, the 4 least significant bits denote the "value" of the corresponding digit, BCD-coded.

Manual control of the gate and delay is still possible. The change from manual to remote operation is accomplished either via the computer again or via an external switch, which is not included in the block scheme.

2.2.2.6.4. High Voltage Control

The output voltage of the Ortec photomultiplier high voltage supply may be controlled externally by applying a DC reference voltage between 0 and 9 Volts to a special connector. This voltage is generated by an analog multiplexer, which acts like a manual step switch on a precise voltage divider chain. The analog multiplexer is controlled by the computer via the above-mentioned multiplexer. Only hundreds and thousands of Volts can be set remotely, which has been decided to be sufficient. Manual remote control of the high voltage is possible, similarly as with the range gate control. Two digits of a four-digit decimal switch are used for this purpose. Precautions are made to avoid the unintentional application of too high a voltage to the photomultiplier tube. If an attempt is made to set the voltage to a value above a limit voltage either manually or by the computer, the voltage is set to zero and an error message is issued to the computer via a combined error line. Error signals from other devices are also transferred through this line. The limit voltage may be changed by a computer-operated switch from 1300 Volts for analog measuring to 2000 Volts for photon counting. After any change of the HV a certain settling time, depending on the amount of the change, is required by the PMT to attain its nominal gain. In order to prevent measurements before the gain has stabilized an error signal is output for a time interval simulated by a R-C network.

2.2.2.6.5 Neutral Filter Wheel Control

As mentioned above, the previously used continuous neutral wedge has been replaced by a filter wheel containing 3 neutral filters with 7.7, 1.5, and .3 % transmissivity, respectively, and one empty hole ("no attenuation" position of the wheel). The wheel is operated by a servo motor. The position of its axis is indicated by a potentiometer connected with it. By applying a logical "1" signal to one of the four input lines (denoted by 0...3 in Fig. 2) of the control unit by the computer, the servo motor moves the wheel to the desired position. An error signal is output as long as the motor is moving. Manual operation is possible by means of a toggle switch with positions 0 - 3 and "ext". In the latter position only remote control is possible.

2.2.2.6.6 Polarizer Control

As the polarization planes of the 694 and 347 nm*) laser beams are perpendicular to each other, the 0°-position of the polarizer for 694 nm is physically the same as the 90°-position for 347 nm, with the angle denoting that between the planes of the polarizer and of the polarization of the incident light. As it was desired to maintain the position of the polarizer with respect to the polarization plane of the transmitted light when the transmitter wavelength is changed, a combined control unit has been developed. A wavelength change thus requires three single operations: Shifting of the frequency doubler into the laser beam path, changing the interference filter and changing the polarizer position. The frequency doubler servo motor has hitherto been operated by a two-position switch at

*) not necessary for remote sensing of stratospheric aerosol

the operating console; the end positions of the doubler carriage have been indicated by two lamps operated by micro switches. The control has now been removed from the console switch to a computer-operated relay in the control unit. When the carriage is moving, i.e. when none of the micro switches is closed, an error signal is output to the computer.

The interference filter wheel has formerly been moved by means of magslips. As the magnetic momentum goes to zero when the wheel approaches the desired position, the positioning is not precisely reproducible. (As mentioned above, the magslip drive for the neutral wedge had been replaced by a servo motor for the same reason). The magslip has been replaced, therefore, by a rotary magnet. This device is operated from the control unit.

The polarizer drive is moved by a DC servo motor, which is stopped by microswitches as soon as one of the two end positions is reached. The motor is operated by the frequency/polarizer control unit which is in turn controlled from the computer via four control lines which are denoted in Fig. 2 by "R", "UV", "0^{o}", and "90^{o}". Applying a logic "one" signal to the "R" line, which means 694 nm (red), the frequency doubler is moved out of the laser beam path, the 694 nm interference filter is moved into the telescope focus and the polarizer either parallel to the polarization plane of the 694 nm incident signal if a "one" is applied to the "0^{o}" line, or normal to it if a "one" is issued to the "90^{o}" line. Accordingly, if a "one" is applied to the "UV" (ultraviolet) line, the frequency doubler is moved into the laser beam, the 347 nm filter into the focus, and the polarizer parallel to the 347 nm plane if a "one" is issued to the "0^{o}" line, or normal to the 347 plane, if a "one" is issued to the "90^{o}" line. The actual position of the polarizer depends, therefore,

on both the polarizer and the frequency control signal from the computer.
The four control signals may also be issued to the control unit manually via pushbuttons.
The electronics for remote control of range gate, high voltage, filter wheels, polarizer and frequency doubler is contained in a 19" chassis.

2.2.2.6.7. Automatic Laser Start

The laser is started by closing a normal-open contact at the laser power supply (cf. description in the previous reports). This contact may now be closed remotely by a relay operated from the computer via interface No. 2.

2.2.2.6.8. External Clock

An external digital clock, synchronized by line frequency, has been developed. The four digits (hours and minutes) are output in BCD code and input to the computer. Two 8-bit channels of one I/O controller are used for this purpose. The clock may be questioned by the computer and the actual time output on punch tape together with the signals. Furthermore, measurements may be started automatically at any time by means of the clock.

2.2.2.6.9. External Stop Pushbutton

An easily accessible "emergency" pushbutton has been installed which gives an interrupt signal to the external interrupt input of one I/O controller. Pressing this button interrupts the current program if the computer interrupt system is enabled (see below). This is used for example when a laser shot is to be repeated because of

superposed spurious pulses.

2.2.2.6.10 Automatic Trigger and Reset of Photon Counter

The automatic background measurement with the photon counter as well as with the transient recorder requires the computer triggering of the photon counter (in the latter case because of the needed range gate start). This is now possible via one of the data output lines from the computer. Simultaneously with the photon counter triggering a pulse is fed through a cable to one of the external trigger input connectors of the transient recorder.

Via another data output line the combined photon counter/peak digitizer unit may be reset externally. This is convenient for analog measurements as in this case the energy monitor data only are needed and the data transfer may be stopped by reset when the peak digitizer readout is completed.

2.2.3. The New Computer Programs

With the availability of the automatic control of the system the development of completely new programs was necessary. As now by means of the floppy disc memory programs can be loaded very quickly into the computer, separate programs for analog and photon counting measurements were prepared. The program for photon counting is briefly described with the aid of Fig. 3.

2.2.3.1. The Photon Counting Program

The flow diagram Fig. 3 presents the new photon counting program. Initially the photomultiplier HV and its limit is set to 2000 Volts. Then the first set of control words for

range gate neutral filter wheel and polarizer position is output from the computer. All control words are contained in a table. After setting the current shot number and other buffers to zero, the measurement is started by triggering the photon counter without firing the laser for background measurement. Since the computer triggering is possible we measure the background in this way instead of using the eleventh or reference channel of the counter which results in an increased accuracy. After triggering the photon counts are transferred to and stored in the computer. Then the laser is started, the counts are again transferred to the computer and the previously measured background subtracted. The "net" counts are output on punch tape in binary format, converted to decimal numbers and displayed on the terminal screen. The net counts are added to the signal buffer contents (which is zero initially) and, with the exception of the first shot, the statistical errors of the accumulated counts are calculated. Then the next measurement cycle is started with the background measurement. The series of measurements with a given range gate and neutral filter setting is stopped automatically if the average statistical error is below 4 %, if 50 single shots have been fired, or manually by means of the fourth computer sense switch. The shot number, sum of energy monitor values, range gate data and time are then output on punch tape, and the range-corrected and energy-normalized partial backscatter profile displayed on the terminal in a semi-log scale, together with the error limits.

The complete series of measurements is now repeated with the following sets of control words until the end of the table is reached. As in the case of analog measuring, the final evaluation of the data is still performed off-line on the main computer with precise plotting facilities.

In general we use a height resolution of 600 m with the

photon counting measurements. The corresponding 4 microseconds gate length per counting channel is included, therefore, in the standard control word table, but may be changed deliberately via the keyboard terminal. The standard altitude intervals and neutral filter settings for the partial measuring series are the following:

Series No.	Altitude Interval (km)	Neutral Filter Attenuation
1	34.8 - 40.8	0 %
2	30.0 - 36.0	0 %
3	25.2 - 31.2	0 %
4	20.4 - 26.4	0 %
5	15.6 - 21.6	92.3 %
6	10.8 - 16.8	92.3 %
7	6.0 - 12.0	98.5 %
8	32.4 - 38.4	0 %
9	27.6 - 33.6	0 %
10	22.8 - 28.8	0 %
11	18.0 - 24.0	0 %
12	13.2 - 19.2	92.3 %
13	8.4 - 14.4	92.3 %
14	3.6 - 9.6	98.5 %

As shown in the table, the complete series of amplitude intervals consists of two parts which are shifted by 300 m with respect to each other resulting in a real height resolution of 300 instead of 600 m. Our examples of backscatter profiles measured by means of the photon counting technique will be presented in part III.2.5. of this report.

2.3. Evaluation of Photon Counting Data

The final evaluation of the photon counting data, which are stored on punch tape, is performed off-line on our main computer facilities utilizing peripheral equipment like fast printer and incremental plotter. Each series of data includes the repeated values of the eleven counting channels and terminates in the value of the sum of the laser output energies (as monitored by the photodiode) and the value of the preset delay. The program of data reduction performs the following steps:

i. Background correction.

ii. Dead time correction. Photons successively striking the photo-cathode of the PMT can only be recorded as separate events if they arrive after minimum intervals. The correction employs an interval of 60 nsec and starts above a minimum number of photons per channel. Thus the linearity of the PMT signal is increased by a factor of about 1.5.

iii. Normalization of the sums of counts per channel to constant number of laser firings and constant laser energy.

iv. Calculation of the root-mean-square error and the standard deviation.

v. Range correction of the backscatter signal and the error limits (multiplication with the square of the height) and logarithmation of these values.

For control purpose the single photon counts as well as the photon sums, normalized values etc., together with channel number and heightscale can be printed as tables by the fast printer.

4 storage sections of the memory contain the height intervals and the logarithms of the range corrected and normalized values of the photon counts and of the upper and lower error limits.

A second part of the program provides for the histogram-like plot of the backscatter values together with error bars versus height. Our 10-channel device (+ 1 channel for background readings) necessitates a stepwise scanning of the atmospheric profile to provide a reasonable resolution. Together with the setting of the delay time the neutral filter wheel must be adjusted since the intensity of the backscatter signal has to be matched with the optimum sensitivity range of the PMT. The plot of the backscatter profile, therefore, will show intensity steps corresponding with the steps of the neutral filter wheel. Usually the whole intensity range of the backscatter signal can be compensated for with a maximum of 3 neutral filter settings. An overlap of 2 channels of the delay ranges and the general trend of the profile (the semilogarithmic presentation of the backscatter signal provides a linear profile of the molecular return) allows the formation of the continuous profile by parallel shift of the profile sections. A second plot then produces the final backscatter profile by readjustment of the zero point of the plotter whenever the neutral filter setting changes.

2.4. Rayleigh Backscatter Profiles

In a second step the lidar backscatter profile must be matched with the calculated Rayleigh (or molecular) backscatter profile allowing the evaluation of the scattering ratio (ratio of the total backscatter to Rayleigh backscatter. On principle we try to combine high altitude probings by lidar with rawinsonde ascents thus providing actual data for the calculation of the expected molecular

returns. But technical reasons sometimes prevent the start of a radiosonde and the question arises to what extent deviate the Rayleigh profiles from each other and can one use a "standard" profile. Fig. 4 presents on the left a number of Rayleigh backscatter profiles calculated from data transmitted by our own rawinsonde. These profiles are separated from each other on the right to allow a discussion of the single curves. The set of curves on the left diverges considerably above 10 km and below 3 km. The presentation on the right shows a parallel shape of some curves above 10 to 12 km. Below about 9 km there seems to exist a seasonal decrease of the slopes between July and January. When having more radiosonde data at hand we shall try to establish criteria which will allow to combine a lidar backscatter profile with a suitable Rayleigh profile if actual radiosonde data are not available. Matching of a certain lidar backscatter profile with anyone of the available Rayleigh profiles can result in a maximum error of the scattering ratio of 12% at 30 km and 20% at 5 km if the matching has been accomplished at 15 km. Employing a "standard" Rayleigh profile which results from averaging the available Rayleigh profiles, can lead to maximum errors of the scattering ratio of 6% at 30 km and 10% at 5 km.

These figures indicate that the lidar data should be related to actual Rayleigh data as far as possible to prevent wrong interpretation of the scattering ratios. If actual radiosonde data are not available a Rayleigh profile must be chosen which corresponds with the given atmospheric conditions.

2.5. Backscatter Profiles

Figs. 5 - 7 give examples of stratospheric backscatter profiles.
The result of the photon counting is plotted in each case

in form of a histogram (with error bar) as a function of altitude. The profile of the molecular backscatter (straight line) calculated from an actual radiosonde ascent serves as reference.

Fig. 5 contains further the analog signal up to a height of 13 km. In Fig. 7 a backscatter profile is plotted in addition, with the position of the polarizer being turned perpendicular to the polarization plane of the emitted light. Compared to the backscatter profile which has been obtained by the parallel turned polarizer, the remaining profile is strongly reduced in its intensity whilst in the range of cirrus clouds values are found which nearly correspond to those which have been found before.

This can be explained as follows:
Whereas practically no depolarization of the emitted strictly linear polarized light takes place with aerosol particles (i.e. not identifiable within the measuring accuracy) a high depolarization is observed with ice particles. Thus backscatter profiles with turned polarizer can be used in making the decision whether the noted backscatter signals are caused by aerosol or ice particles.
This question is of particular importance in the case of backscatter profiles from the tropopause level.

3. The Ozone Measuring Program

The balance of the tropospheric ozone, the source of high ozone concentrations in rural areas, the exceeding of national ambient air quality standards by natural, not anthropogenic events, and the influx of ozone from the stratosphere during stratospheric intrusions, these all are nowadays questions of high topicality which are discussed on a broad scale.
In order to contribute to a solution of the questions in-

volved in this subject it is planned to take up measurements of ozone concentration - supplementary to the measurements at the Zugspitze - also at the stations Wank (1800 m a.s.l.) and Garmisch (740 m a.s.l.). The instruments needed for this purpose could be procured during the reporting period. The preliminary technical works at the two additional stations have been largely concluded.

Experiences gained from ozone measurements at the Zugspitze have shown that a relatively great amount of technical effort is necessary if continuous measurements shall be guaranteed. High demands are placed on the calibration of the measuring instruments to ensure the comparability of data which will be evaluated lateron in form of a balance. For this reason the following maintenance schedule has been set up:

All the three stations are equipped with the same unit type (ECC-Meter Model 005, manufacturer Astro Engineering). A fourth instrument working according to the same method (ECC-Meter Model 002) is always kept ready for operation in order to serve as stand-by unit in case of a failure of one of the instruments employed at the stations. Earlier experiences revealed that the measuring cells of the chemoelectric ozone instruments show certain symptoms of aging if operated longer than 6 months (e.g. decrease of sensitivity). However, these effects can be avoided if the respective cells are carefully cleaned and newly activated after a relatively short period of operation. A second cell for each instrument is therefore kept available in the laboratory. The cells are always exchanged after 3 weeks of operation, the used cells are attended in the laboratory and kept there with an aqua-bidest filling until the next operation. This frequent exchange of the measuring cells proved a full success.

Since only after elaborate calibration of all units employed

the obtained measuring series can be compared among each other which is, however, a necessary requirement for the aimed-at balance of the tropospheric ozone, the laboratory was generously equipped with calibration facilities.

A chemoluminecence unit (Ozone Monitor 8002, manufacturer Bendix) is available for short-time parallel measurements to check on the performance of the instruments which are in routine use.

A further unit (type 779, manufacturer Schenk & Koller) working likewise according to the potassium-iodide method is used as laboratory standard unit. This unit is particularly suited as standard unit because the electrodes can be removed. Hence it is possible to restore the electrodes after use to their original condition by suitable cleaning procedures (annealing of the platinum anode, electrolytic cleaning of the silver cathode). A digital display is a further advantage of this unit in that it permits a fast reading during the calibration process.

A standard gas generator (manufacturer Bendix) serves as ozone source during the calibration procedure. The ozone is generated by UV-radiation on a pre-cleaned zero air flow. The UV-lamp of this instrument is supplied by adjustable constant current. Constant gas flow is ensured by temperature-controlled capillary tubes. The ozone concentration produced by the ozone generator is determined by a modified wet-chemical method (KJ-method).

The usual methods described in the literature proved to be unsuited as in this manner just poorly reproducible values could be obtained. The buffered neutral or slightly acid KJ-solutions were found to be extremely sensitive to varying laboratory conditions. So, for instance, air-oxidation and oxidation by sunshine was observed. These interferences could be avoided by the use of alkaline KJ-solutions.

A further source of interference in the wet-chemical calibration lies in the instability of the commonly used reference solutions. Both highly diluted iodine solutions and potassium iodate solutions can only be used for a short time. Different results are obtained even in the course of one day.

The usual colouring with starch indicator solution (needed for photometer measurements at 352 nm wavelength) proved to be impractical, too. Whereas the unexposed samples always assumed a violet colour. This different colouring obscured the results.

These difficulties could be overcome in that an alkaline potassium permanganate solution was used as reference solution. This solution is extremely stable over a long period of time and has in an alkaline potassium iodine solution the same oxidizing effect as in the ozone as apparent from the following reaction equation:

$$3\ O_3 + 6\ KJ + 3\ H_2O \longrightarrow 3\ O_2 + 6\ KOH + 3\ J_2$$

$$2\ KMnO_4 + 6\ KJ + 4\ H_2O \longrightarrow 2\ MnO_2 + 8\ KOH + 3\ J_2$$

Hence 2 $KMnO_4$ correspond to 3 O_3 and so any desired ozone concentration can be simulated by potassium permanganate solutions. Calibration is done in the following way:

The photometer is calibrated with several potassium permanganate reference samples. The air with different ozone content produced by the generator is transferred through two series-placed impingers containing KJ-solution. The iodine liberated by oxidation with the ozone is measured by the photometer and the ozone concentration is determined by comparison with the reference samples. The colouring with starch has become superfluous since the extinction by the liberated iodine can reproducibly be determined even at 576 nm wavelength (light source: Mercury vapour lamp).

Calibration procedures according to this principle are carried through every three months.

IV. GRAPHICAL REPRESENTATION OF FALLOUT AND COSMOGENIC RADIONUCLIDES OF AUGUST 1975 THROUGH SEPTEMBER 1976

Fig. 8 shows the time variations in the concentrations of the fallout and the radionuclides Be7, P32, P33 and S35. Moreover, the daily means of ozone, measured at the Zugspitze, and the daily precipitation rates are depicted in the Figure.

After a number of minor failures at the measuring instrument the measurements of ozone concentration had to be interrupted temporarily in March 1976. Owing to some constructional alterations at the measuring station the measurements could be resumed only in October 1976 (results are no more presented in this Figure).

A marked annual variation can be identified for none of the measured quantities during the reporting period. The month of January is that with the lowest concentration of cosmogenic radionuclides. During the rest of the time the values vary more or less strongly about constant mean values.

Three distinct peaks in the concentration of the nuclides Be7, P32 and P33 are indicative of a very intense stratospheric intrusion: 23.11.1975, 4.3.1976, and 28.4.1976. The first case will be discussed in some detail in Chapter V. Obviously, during this stratospheric intrusion, also ozone of stratospheric origin penetrated into the lower troposphere.

V. APPLICATION OF A FORECASTING TECHNIQUE FOR STRATOSPHERIC INTRUSIONS TO THE EARTH SURFACE AND CRITICAL EXAMINATION OF THE FORECASTING QUALITY

1. Forecasting of Stratospheric Intrusions

As presented in Annual Report Part VI a method was developed permitting the forecasting of an influx of stratospheric air into the biosphere by observation of the relative humidity in the upper and middle stratosphere. In the present report a test is offered verifying subsequently the forcecasting accuracy.

2. First Attempts at a Forecasting of Intrusions of Stratospheric Air

Since October 1975 daily internal prognoses of the probability of intrusions of stratospheric air are issued for the following days. These prognoses are based on the measuring data of the radiosonde ascents conducted by the German Weather Service in Munich-Riem at 00.00 GMT and 12.00 GMT. The data are received by teletype and are actually evaluated by computer. These evaluations constitute the basis for our prognoses.

3. Tentative Result of the Practical Application of a Forecasting Technique of Injections of Stratospheric Air to the Earth's Surface

3.1. Data Used

The injection of stratospheric air to the earth's surface (in our case Zugspitze) is indicated by a striking increase

in the concentration of stratospheric radionuclides. This detailed investigation is limited to Be7 concentration.

The radiosonde ascents of the station Munich-Riem serve as meteorological basis. The two daily temp-telegrams are received in the morning and are immediately evaluated by computer. The vertical profile of the relative humidity as well as of temperature is an essential factor in the corroboration of the prognoses. This will be specified later by an example. The forecast is noted down daily and then, several days later, compared against the actually determined concentration values of the Be7 indicating injections of stratospheric air.

3.2. Results

Fig. 9 shows the variation of the concentration of the Be7 during the last 3 months of the year 1975, that means since the beginning of the experimental period. It represents the background of the Gamma-spectrometer and the total count rate (Be7 activity + background). We immediately note a strong fluctuation of the Be7 concentration and relatively frequently occurring peak values indicating an injection of stratospheric air.

For a verification of the forecasting accuracy the following prognostic levels and the measured concentration levels of the Be7 have been defined in Tables 4 and 5 of Annual Report Part VI.

In Fig. 10 the forecasting levels are plotted in pairs against the actually determined concentration levels throughout the experimental period. Excellent agreement would be reached in case both columns of each pair would show an equal height. Good conformity is in fact observed between the forecasting-columns (dashed line) and the

concentration columns: as a rule high concentrations as well as very low concentrations are indicated with great accuracy.

Table 4

Classification of the Measured Be7 Concentration in 6 levels

Be7 Concentration x 10^{-2} pCi/m^3	Level
2.9	0
3 - 5.9	20
6 - 9.9	40
9 - 11.9	60
12 - 24.9	80
25	100

Table 5

Forecasting Levels of Be7 Concentration

Definition	Level
very low	0
low	20
mean	40
high	60
peak value	80
extreme peak	100

Table 6

Verification Rate of Deviation A Between Prognosticated and Measured Activity of Be7

Deviation A in Levels of 20 Units	Verification Rate in %	Forecasting Quality
0	27	optimal
20	47	very good
40	18	moderate
60	8	bad
100	0	very bad

Table 6 represents an evaluation of the forecasting accuracy. Forecasting quality is indicated by the deviation between actually determined relative activity (according to scale 0 - 100) and the prognosticated activity. Here again different levels are used:
"Deviation 0" means complete conformity, "deviation 20" means that according to our scale a difference by 20 units existed between prognostic and actual relative concentration, etc. It is apparent from Table 6 that with strongest probability a deviation by 20 units is found, with next following probability a deviation by 0 units, and with very little probability by 40 and 60 units. Deviations by 100 units were not observed. Considering "deviation 0" and "deviation 20" to be adequate for practical application, so it follows that this result is obtained at 74 % of all cases. Extremely bad prognoses were found only at 8 % of all cases, completely wrong prognoses were not observed.

3.3. Representation of a Characteristic Individual Case of a Strong Injection of Stratospheric Air

Fig. 9 represents the period from 20 through 27 November 1975 indicated by a horizontal bar. A steep increase of Be7 radioactivity is observed in the period from 22 through 23 November, the maximum value was recorded on 24 November. Based on the data of radiosonde ascents of the station Munich-Riem, Fig. 11 shows the variation in time of the vertical profile of the relative humidity along with wind direction and wind speed. Following is a systematical subsidence of a dry air body, with the dry air parcel penetrating Zugspitze level between 00.00 GMT and 12.00 GMT on 23 November. This is also apparent from the relative humidity recorded at Zugspitze station itself. The vertical bars indicate strong inversions of temperature caused by the process of subsidence. On 24 November the Zugspitze station is located within the extremely dry air layer with a relative humidity of less than 10%. The extremely high concentration of Be7, only gradually decreasing towards 26 November, is simultaneously recorded inside this air body. This graph shows very clearly the variation in time of a strong intrusion of stratospheric air from the range of tropopause (tropopause altitude marked by heavy dots in Fig. 11). Daily recordings of the two-dimensional humidity distribution - as shown in Fig. 11 - constitute the practical basis for the deriving of the forecast. In this case a strong injection of stratospheric air was rather likely to be expected already on 22 November between 00.00 GMT and 12.00 GMT. From the deriving of the forecast until the reaching of the maximum value of the Be7 concentration 48 hours will elapse. This is the average time lag between the deriving of the forecast and the arrival of the event.

3.4. Prognosis of Fresh Fallout After a Chinese Nuclear Weapon Test

The influx of fresh fallout after the Chinese nuclear weapon test of 25.9.1976*) has been chosen as a further example of the applicability of our method to prognosticate stratospheric intrusions.

Fig. 12 shows in part a the time variation of the Be7 concentration during the period after the 25th of September 1976. Part b shows the beta activity of the fallout during the same period. Two periods with an influx of stratospheric air can be identified through the Be7-concentration (05.10. - 11.10 and 21.10. - 25.10.). As can be seen from the parallelism with the fallout activity, both intrusions of stratospheric air were contaminated with fresh fallout. Investigations by gamma spectrometry verified this observation. An analysis of the northern hemispheric flow conditions revealed that the fallout peaks of 8 and 11 October occurred during the first rotation of the fallout cloud and the peak of 23.10. during the second rotation as it is apparent from the graphical representation in part c of Fig. 12.

Parts d and e of Fig. 12 illustrate how the forecasting method is applied. The upper section (part d) reflects the time variations of the humidity profiles, the lower section the prognosticated influx intensities derived from them. In view of the development on 3 and 4 October, a medium to high influx intensity has been expected for the period until the 5th of October. However, as the influx

---

*) Although the event took place right after the end of the reporting period it has been anticipated in this report since is striking character is well suited to demonstrate the effectiveness of the forecasting method

did not approach the measuring station level no higher activity was found in the air.

On the other hand, precipitation was setting in during said period in which high concentrations of fallout were found obviously as a result of a washout process caused by the development of precipitation at an altitude of 4 - 8 km. The fallout in the air reached the measuring station only on 6th October with a second influx of stratospheric air, this time breaking down as far as to ground level. Highest influx intensity has been prognosticated for this day.

A similar pattern is found with the influx between 21.10. and 25.10. Beginning on 21.10. at high altitude, the influx progresses to ground level until the 23rd of October. Again, highest influx intensity has been prognosticated for the 22nd and 23rd of October which is in absolute agreement with the measured activities.

VI. FALLOUT ANALYSIS AFTER THE CHINESE NUCLEAR WEAPON TEST OF SEPTEMBER 1976

In Annual Report Part VI we described in detail a Gamma-Spectrometer with GeLi-detector suitable to conduct actual monitoring of fallout with regard to concentration and composition. The passing of the fallout cloud after the Chinese nuclear test gave rise to an actual application of the instrument.

Fig. 13 shows for the 3 stations Zugspitze, Wank and Garmisch the time variation of the total beta activity after ignition of the nuclear weapon. The data were obtained from short-term (4 per day) filter expositions which commonly are made to determine the natural radioactivity from soil emanation. The activity of heavy metal precipitation in aerosol samples taken within the scope of

the present study is plotted in the upper line of the picture. At all stations two intervals with enhanced radioactivity (at the Zugspitze even three intervals) can be identified between 6 and 12 October.
A further event about the 24th of October is essentially more smoothed, the noted activity values are less high but more persistent. This fallout event may be attributed with certainty to the second hemispheric rotation of the fallout cloud. Through the immediate employment of the Gamma-Spectrometer it has been possible to identify in both precipitation and aerosol samples the following fresh (short-lived) fission products:

Nuclide	Half-life
Mo 99	2.7 d
Te 132	3.2 d
J 131	8.0 d
Nd 147	11.1 d
Ba 140 with La 140 daughter	12.8 d
Ce 141	32.5 d
Zr 95 with Nb 95 daughter	65 d

These figures show some gamma-spectra from the time about 6 October 1976.

VII. INFLUENCE OF THE STRATOSPHERIC-TROPOSPHERIC EXCHANGE ON THE TROPOSPHERIC OZONE

With the cooperation of Professor Dr. Elmar R. Reiter of the Department of Atmospheric Sciences, Colorado State University, Fort Collins, Colorado, a joint paper on the question of the origin of the tropospheric ozone has been published. A reprint of the paper is found on the pages following.

Arch. Met. Geoph. Biokl., Ser. A, 26, 179–186 (1977)

ARCHIV
FÜR METEOROLOGIE
GEOPHYSIK UND
BIOKLIMATOLOGIE

551.510.4

Department of Atmospheric Science, Colorado State University, Fort Collins, Colorado, U.S.A. and Institute for Atmospheric Environmental Research of the Fraunhofer Gesellschaft, Garmisch-Partenkirchen, German Federal Republic

Lower-Tropospheric Ozone of Stratospheric Origin *

E. R. Reiter, H.-J. Kanter, R. Reiter, and **R. Sládkovic**

With 3 Figures

Received May 4, 1977

Summary

Using hourly ozone concentration data from Zugspitze Observatory, of the Institute for Atmospheric Environmental Research, Garmisch-Partenkirchen, Germany, it is shown that under a propitious superposition of stratospheric and tropospheric flow patterns U.S. Federal maximum ozone standards of 80 ppb can occasionally be exceeded by a factor of two or more in the lower troposphere. Further dilution of these concentrations has to be expected by mixing processes in the planetary boundary layer.

Zusammenfassung

Niedertroposphärisches Ozon stratosphärischen Ursprungs

Stündliche Ozonkonzentrationswerte vom Zugspitzobservatorium des Institutes für Atmosphärische Umweltforschung, Garmisch-Partenkirchen, Bundesrepublik Deutschland, zeigten, daß bei einer günstigen Überlagerung von stratosphärischen und troposphärischen Strömungsfeldern die in den USA vorgeschriebene, einstündige Maximalkonzentration von 80 ppb unter Umständen um mehr als einen Faktor 2 in der unteren Troposphäre überschritten werden kann. Eine weitere Verdünnung dieser Konzentrationen kann durch die Mischungsprozesse in der planetaren Grenzschicht erwartet werden.

In several previous reports [2, 3, 4] we have compared daily-mean ozone concetrations to daily fallout of nuclear bomb debris or of cosmogenic radionuclides. From such comparisons it appeared that the daily mean values of O_3 at ground level stayed below 50 per cent of the federally established

* Research reported in this paper was supported by ERDA Grant E(11-1)-3425 to the Institute for Atmospheric Environmental Research, Garmisch, and by EPA Contract No. 68-02-2084 to the Stanford Research Institute, Menlo Park, California.

maximum value of 80 ppb. Daily mean values of ozone measured at the peak of Zugspitze Mountain, Germany (3000 m above mean sea level) were at a maximum range of 50 to 60 ppb during approximately 2.5 percent of the days with observations. Since additional mixing between the 3000 m level and the valley floor is to be expected, the measurements at Zugspitze agreed well with our estimates of O_3 concentrations based upon radioactive fallout concentrations.

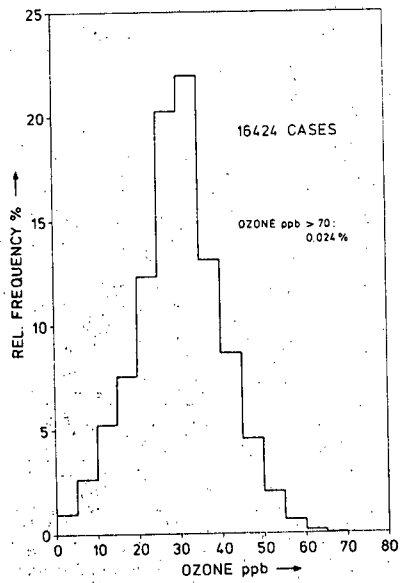

Fig. 1. Per cent frequency distribution of mean hourly ozone concentrations (ppb), August 1973 to February 1976. Eight hours in excess of 80 ppb (see Table 1) produced a frequency of 5×10^{-4} per cent, too low to register on this diagram

One problem which could not be solved with previously available data was to estimate the probability of hourly mean ozone concentrations to exceed the hourly federal maximum level. One has to assume that hourly ozone concentrations vary about the daily mean value. A relatively high daily-mean concentration, therefore, produces a certain chance that during one or several hours the federal maximum value of 80 ppb was, indeed, exceeded. Ozonsonde observations over North America revealed that in 0.2 per cent of the available cases ozone concentrations of stratospheric origin within the planetary boundary layer exceeded the federal standards. Unfortunately, no

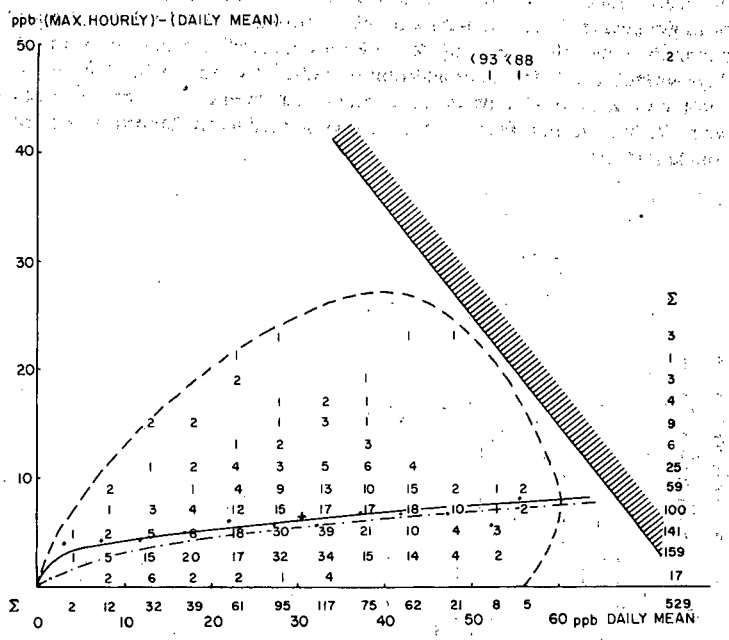

Fig. 2. Difference between maximum hourly ozone concentrations (ppb) and daily mean concentrations as a function of daily mean concentrations, observed at Zugspitze (3000 m above M.S.L.) between August 1973 and February 1976. The frequency distribution by 5-ppb classes of daily mean and 2-ppb classes of hourly maximum minus daily mean is given gy the numbers in the diagram. The dashed line indicates the limits of the present data distribution. To the right of the shaded line the federal maximum value of 80 ppb would be exceeded. Dots indicate the mean values of (max. hourly-daily mean) in each class of daily mean values. The solid line gives an approximate best fit to these dots. The cross marks the mean value of both distributions, that of (max. hourly – daily mean) and that of the daily mean values. The dashed-dotted line approximates the position of the mode values in each class of daily mean concentrations. Note that two observations fall outside the plotted distribution

hourly surface observations were available to determine if the mixing processes near the ground, and the resulting destruction of ozone, still produced excess values during one-hour periods. Similar reservations hold for a case of O_3 concentrations more than twice as high as the federal standards, observed over Albuquerque, New Mexico, on 25 March 1964 above the 500-mb level. Strong chinook winds could bring parcels of this air mass to the ground without appreciable dilution, producing short-term "spikes" in the temporal

variation of O_3 concentrations. It is to be expected, however, that the averaging process, even over one-hour periods, would reduce these excessive instantaneous concentrations by approximately a factor of two.

In order to explore the probability of excessive one-hour ozone concentrations more thoroughly, hourly ozone observations were obtained from Zugspitze Observatory (3000 m above M.S.L.) of the Institute for Atmospheric Environmental Research of the Fraunhofer Gesellschaft, Garmisch-Partenkirchen, West Germany [8, 9, 10, 11, 12]. Fig. 1 contains a frequency distribution of hourly ozone concentrations by season, expressed in ppb.

Fig. 2 shows in graphical form the distribution of daily one-hour maximum O_3 concentrations in relation to the daily mean values of ozone (in ppb). To the right of the slanting shaded line the federal maximum value of 80 ppb would have been exceeded.

This diagram reveals that under the "normal" behavior of maximum one-hour concentrations the federal value of 80 ppb should not be exceeded during more than perhaps 0.05 percent of days, i. e., perhaps once in 2000 days, or once in four times the sample length represented by this diagram. This „normal" behavior is dictated by the transport and mixing processes prevailing in the upper and middle troposphere and, especially in the range of relatively high daily-mean values, by intrusions of stratospheric air into the lower troposphere.

Two days, January 8 and 9, 1975, departed significantly from this "normal" behavior, yielding maximum one-hour concentrations of O_3 in excess of 145 ppb. (The instrument, on these occasions, registered off scale). The hourly O_3 values for these two days are reproduced in Table 1. Our first inclination was to discredit these measurements as having been subject to instrument malfunction. After closer scrutiny of other evidence we are, however, prepared to accept these values as realistic. The following facts had to be considered:

Table 1. *Hourly Ozone Concentrations (ppb), Zugspitze on January 8 and 9, 1975*

Time	January 8	January 9	Time	January 8	January 9
1 hr.	25.82 ppb	> 145 ppb	13 hr	42.88 ppb	32.12 ppb
2	27.28	> 145	14	50.81	32.22
3	27.94	> 145	15	62.21	25.61
4	30.08	> 145	16	52.92	25.18
5	31.30	81.33	17	52.06	24.88
6	30.93	28.50	18	54.83	22.37
7	28.07	25.33	19	57.03	22.39
8	27.37	27.79	20	62.80	19.84
9	26.91	30.31	21	79.85	19.10
10	27.69	30.71	22	114.10	17.92
11	37.78	31.43	23	> 145	16.89
12	47.88	31.82	24	> 145	17.17

1) The hourly O_3 concentrations on these two dates do not behave spuriously but reveal an increase from, and later a decrease to, the usual levels of O_3 concentrations observed at Zugspitze.
2) Within the available sample, these two days constitute 0.4 per cent. Since the excessive concentrations straddled the midnight hours they should actually be counted as only one case, or one day, i. e., 0.2 per cent of the available sample. Such a frequency of occurrence is in excellent agreement with our data from the North American ozonesonde network.
3) The daily average Be-7 concentrations measured at Zugspitze showed the following trend:

Jan. 1975	7.	8.	9.	10.	11.	12.	13.	14.	15.	16.	17.	18.
pc/m^3	1.33	4.99	10.35	13.79	11.17	11.66	14.60	11.84	15.29	7.10	5.71	2.98

Be-7 is produced by cosmic radiation mainly in the lower stratosphere [6], hence can serve as tracer for stratospheric air intrusions into the troposhere. The increase in Be-7 concentrations between 8 and 9 January suggests such an influx of stratospheric air. The ozone increase on 8 January is not matched correctly in the Be-7 data because of differences in sampling time.
4) The weather maps issued by the German Weather Service, Offenbach, show the passage of a cold front with precipitation and a strong jetstream, even at the 500-mb surface, early on January 8. A short-wave trough which, on January 7, 00 GMT, was over the North Sea, passed the Alps by January 7, 00 GMT. Such a weather situation is conducive to import of stratospheric air into the lower troposphere, as discussed in a previous report [5].
5) The 200-mb surface, indicative of conditions in the lower stratosphere, reveals a rather unusual configuration of planetary wavenumber two. Usually this wavenumber is characterized by a trough over East Asia and another trough over North America. The situation leading up to the events of January 8 and 9, 1975, is dominated by a planetary long-wave trough over eastern Eruope, which began to establish itself on January 6. Relatively warm temperatures in the trough axis at 200 mb, and colder temperatures to the west of this axis, suggest the presence of sinking motions in the lower stratosphere within the northwesterly flow to the rear of the trough. The 100-mb maps for this period (Fig. 3) show that the center of gravity of the polar vortex, i. e., its lowest geopotential heights at this pressure level, is located over the European sector. This, again, is a rather unusual configuration.
Thus, the abnormal location of an exceptionally strong trough in the stratosphere over Europe, with sinking motions on its rear side, would help to move ozone from the middle to the lower stratosphere in unusually large amounts over this region. The low-stratospheric ozone reservoir – replenished by the downward motions in the stratosphere – was "tapped" by a typical

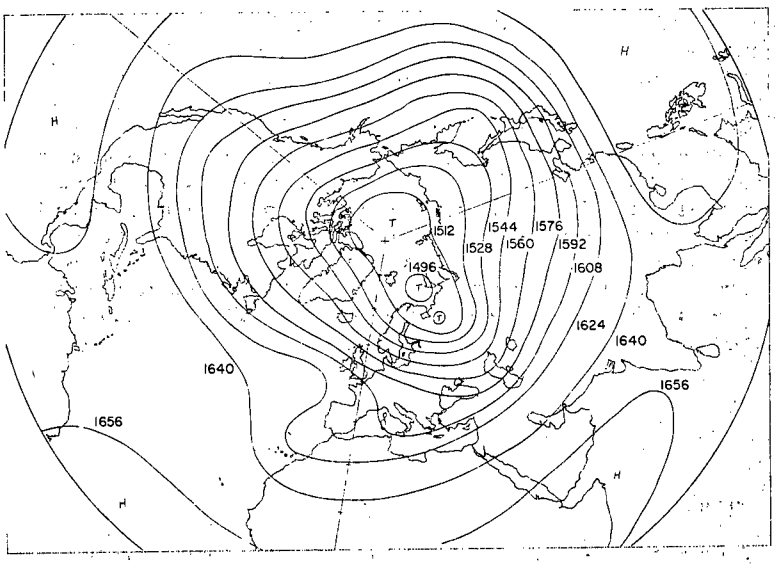

Fig. 3. 100-mb map, 7 January 1975, 00 GMT (Täglicher Wetterbericht, Deutscher Wetterdienst, Offenbach)

intrusion event connected to a strong jet stream and to an advancing cold front. The sequence of these events led to the observed, abnormally high, ozone concentrations on Zugspitze Mountain on January 8 and 9, 1975. At the present, we are inclined to argue that the mis-match of these two days to the rest of the statistical sample, revealed in Fig. 2, is due to the anomalous stratospheric flow pattern, rather than to an unusual state of mixing and transport processes in the upper troposphere. Large-scale vertical transport processes in the lower stratosphere could easily produce ozone concentrations above the tropopause which are more than twice as high as seasonally averaged values with "normal" flow patterns (see [1, 7], for corroborating data).

The climatological mean long-wave trough position in the winter stratosphere of North America would tend to produce O_3 concentrations in excess of the federal standard value of 80 ppb by a factor of two to three, somewhat more often than over Germany. The situation over Albuquerque on 25 March, 1964, should be considered typical of such an event. Strong dilution to less than half of the concentrations encountered in layers embedded in the middle troposphere should be expected as mixing processes in the planetary

boundary layer take over. Even though short-term "spikes" of O_3 concentrations can approach the values in the layers which are being "tapped" by turbulent exchange processes, and should be expected to occur with durations of several minutes, concentration values averaged over one-hour intervals at the ground (not counting mountain peaks like Zugspitze) should be less than half of the values encountered in layers located above the planetary boundary layer. If we ascribe maximum concentrations of two to three times in excess of federal standards to such elevated layers, federal standards would be exceeded on rare occasions at the ground. These occasions would be tied to the cyclogenetically active locations of middle latitudes, and to regions over which the stratospheric long-wave trough pattern is able to establish an above-normal reservoir of ozone concentrations in the layers above the tropopause.

References

1. Reiter, E. R.: Atmospheric Transport Processes, Part 2: Chemical Tracers. U. S. Atomic Energy Commission, Division of Technical Information, TID-25 314, 382 pp., 1971.
2. Reiter, E. R.: The Transport of Radioactive Debris and Ozone From the Stratosphere to the Ground. Report to Stanford Research Institute, 36 pp., 22 November 1975.
3. Reiter, E. R.: On the Correlation Between Cosmogenic Be-7 and Ozone. Report to Stanford Research Institute, 19 pp., 23 December, 1975.
4. Reiter, E. R.: Significance of Stratospheric Ozone for Ground-Level Ozone Concentrations. Report to Stanford Research Institute, 15 pp., 17 April, 1976.
5. Reiter, E. R.: Ozone Concentrations in the Lower Troposphere as Revealed by Ozonesonde Observations. Report to Stanford Research Institute, 106 pp., 26 March, 1976.
6. Reiter, E. R., W. Carnuth, H.-J. Kanter, K. Pötzl, R. Reiter, and R. Sládkovic: Measurements of Stratospheric Residence Time. Arch. Met. Geoph. Biokl., Ser. A, *24*, 41–51 (1975).
7. Reiter, E. R., E. Bauer, and S. C. Coronitti: The Natural Stratosphere of 1974, Department of Transportation, Washington, D. C. 20590, 1975.
8. Reiter, R.: Durchbrüche stratosphärischer Luft zur Erdoberfläche – Ein Beispiel für angewandte atmosphärisch-physikalische Forschung. Umschau, *72*, 429–431 (1972).
9. Reiter, R., R. Sládkovic, K. Pötzl, W. Carnuth, and H.-J. Kanter: Studies on the Influx of Stratospheric Air Into the Lower Troposphere Using Cosmic-Ray Produced Radionuclides and Fallout. Arch. Met. Geoph. Biokl., Ser. A, *20*, 211–246 (1971).
10. Reiter, R., R. Sládkovic, H.-J. Kanter, W. Carnuth, and K. Pötzl: Measurement of Airborne Radioactivity and Its Meteorological Application, Part IV. Annual Report, AEC Document No. NYO-3425-10, 61 pp, 1975.

11. Reiter, R., H.-J. Kanter, R. Sládkovic, and K. Pötzl: Measurement of Airborne Radioactivity and Its Meteorological Application, Part V. Annual Report, ERDA Document No. NYO-3425-12, 86 pp., March, 1976.
12. Reiter, R., H.-J. Kanter, R. Sládkovic, and K. Pötzl: Measurement of Airborne Radioactivity and Its Meteorological Application, Part VI. Annual Report, ERDA Document No. NYO-3425-14, March, 1977.

Authors' addresses: Dr. Elmar R. Reiter, Department of Atmospheric Science, Colorado State University, Fort Collins, CO 80523, U. S. A., and Dr. H.-J. Kanter, Dr. Reinhold Reiter and Dr. R. Sládkovic, Institute for Atmospheric Environmental Research of the Fraunhofer Gesellschaft, Garmisch-Partenkirchen, West Germany.

Printed in Austria

VIII. SOLAR TERRESTRIAL RELATIONSHIPS

Supplementary to the comprehensive statistical processing of a 5-year observation sequence a harmonic analysis was performed on the basis of the Be7-data in order to examine whether periodicities can be found in agreement with the solar rotation.

Geophysical parameters being subject to solar influences reflect as a rule a periodicity which is more or less commensurate with the frequency of solar rotation (27 days at the solar equator, 28.5 days in $\pm$ 30° latitude). Since BARTELS this behavior has long been known of the geomagnetic activity, but also of radio propagation and others. So it was an obvious idea to conduct a harmonic analysis of the daily mean concentration of Be7 in order to find out whether this would reveal a frequency in agreement with the solar rotation.

Due to computer memory limitations the data series had to be divided into two periods: November 1969 - July 1972 (984 values) and July 1972 - January 1975 (953 values). In some cases relative concentrations were considered. In these cases consecutive sets of 32 concentration values were averaged (to form a kind of formal "monthly" mean concentration) and the concentration values were replaced by their ratio to the corresponding mean concentration.

The computations follow the procedure described in PANOFSKY and BRIER [1].

There are essentially three steps:

a) M + 1 autocorrelation coefficients are calculated using the formula

$$r_L = (S_X^2 N)^{-1} \sum_{i=1}^{N} (X_i - \bar{X})\,(X_{i+L} - \bar{X}),\ L = 0,\ldots M$$

with mean value

$$\bar{X} = N^{-1} \sum_{i=1}^{N} X_i$$

and variance

$$S_X^2 = N^{-1} \sum_{i=1}^{N} (X_i - \bar{X})^2$$

Here X_i stands for the daily Be7 concentration (or relative concentration), M is the maximal lag and N the "window width" given by the difference of the total number of data available minus the maximal lag (in order to allow shifts).

b) The set of autocorrelation coefficients is supposed to be an even function of time that can be expressed by a Fourier series containing cosines only. The spectral intensities are computed according to

$$B_i = M^{-1} \left(r_o + 2 \sum_{L=1}^{M-1} \left(r_L \cos\left(\pi \frac{iL}{M}\right)\right) + (-1)^i r_M\right),\ i = 0,1\ldots M.$$

For i = 0 and i = M the B_i have to be divided by two in order to get the correct spectral intensities.

c) The spectral intensities B_i are replaced by smoothed values

$$S_i = 0.25\, B_{i-1} + 0.5\, B_i + 0.25\, B_{i+1},\ i = 1,2,\ldots M-1,$$

$$S_o = B_o \quad \text{and} \quad S_M = B_M.$$

These smoothed spectral intensities S_i are plotted versus the frequencies $v_i = i/2\,M\Delta t$. Δt is the time difference between two data points X_i and X_{i+1}, in our case $\Delta t = 1$ day.

Fig. 18 shows such a smoothed spectrum for the autocorrelogram of the daily mean concentrations of Be7 for the measuring period November 1969 to July 1972. Fig. 19 shows a similar spectrum of daily relative Be7 concentrations for the period July 1972 to January 1975. In both cases, the maximal lag in establishing the autocorrelogram is 511 days.

From both data groups - as illustrated in Figs. 18 and 19 - the frequencies specified in the following table are accentuated out of the noise, the technically-dependent dividing into two data groups leading even to a mutual confirmation of the main frequencies found.

Table

Length of the Period in Days for the Following Time Intervals

Nov. 1969 - July 1972	July 1972 - Jan. 1975
4,7 +	5,2 +
6,5	7,1
10,3 +	11,6
20,9 +	18,9
23,2	24,0
30,5 +	30,1 +

+ very distinct

The particularly salient period with 30 days rather approaches the rotation frequency of the sun (mainly if

we consider it for about $\pm$ 30° latitude). An exact and over a longer period stable coupling between solar rotation and geophysical parameters can hardly be expected, especially not if the sector structure of the interplanetary magnetic field is assumed to be the triggering factor because a) the number of the sector boundaries changes with time (mostly between 2 and 4) and so does the position of the irregular boundaries on the sun, consequently, b) also higher frequencies will occur which - just as the rotation fundamental frequency - c) change their phase position depending on whether the active centers on the sun increase or decrease in intensity. This means that we may expect also shorter, solar-dependent lengths of periods. Hence it is just possible that the phase-lengths found between 24 and 10 are caused by solar action.

Not at least it must be remembered that the concentration of Be7 in the troposphere is not only modulated by variations of the intensity of the stratospheric influx, but also by processes eliminating the Be7 out of the air - first of all by precipitation. Therefore it is interesting to note that the frequency analysis yields a very well defined length of period extending over 4,7 - 5,2 days. It is in full accordance with the known mean frequency of the cyclonic activity above Europe. Interesting in this connection are also the investigations of GEISLER and DICKINSON [2] who found a global five-day wave in conjunction with zonal winds, and another study of RODGERS on the existence of a five-day wave in the upper stratosphere [3]. At the same time reference is made to the analysis of the variability of hemispheric scale energy parameters by McGUIRK, REITER, and BARBIERI [4].

References

[1] Panofsky, H.A., and G.W. Brier:
Some Applications of Statistics to Meteorology.
Chapter VI. University Park, Pennsylvania (1968)

[2] Geisler, J.E., and R.E. Dickinson:
The Five-Day Wave on a Sphere With Realistic Zonal Winds.
J. Sci., 33, 632 - 641 (1975)

[3] Rodgers, C.D.:
Evidence for the Five-Day Wave in the Upper Stratosphere.
J. Atmosph. Sci., 33, 710 - 711 (1976)

[4] McGuirk, J.P., E.R. Reiter, and A.M. Barbieri:
On the Variability of Hemispheric Scale Energy Parameters.
Envir. Res. Papers, Fort Collins (1975)

IX. CONCLUSIONS

The works under contract led to the following results or conclusions respectively:

Computerized, fully automatic lidar systems make it possible with very high resolution regarding time and distance (or height resp.) to determine aerosol structures and to study their variations.

The method used for single photon counting proved to be completely suitable for the performance of routine monitoring of the relative aerosol backscatter in the stratosphere up to 35 km.

For an exact interpretation of the stratospheric backscatter profiles, however, it is necessary to acquire atmospheric density data in order to be able to compute as precisely as possible the profile of the molecular backscatter. The use of standard atmospheres can lead to essential errors in the determination of aerosol backscatter profiles.

The statistical investigations described above, as well as the actual example presented to demonstrate the application of the forecasting method permit the conclusion that a prognosis of the influx of stratospheric air can be satisfactorily performed by the observation of the time variation of the relative humidity in the upper troposphere. First attempts have shown that the results presented can still be improved by a more intensive parameterization.

Under certain weather conditions stratospheric ozone can be transported into the lower troposphere by intrusions of stratospheric air. The ozone concentrations observed during such events can considerably exceed federally established maximum values (e.g. US Federal Maximum Ozone Standard).

Harmonic analyses of the frequency distribution of the Be7 concentrations result in frequencies which allow the reasonable assumption of a periodic triggering of the stratospheric-tropospheric exchange by solar activity.

X. FUTURE PLANS

1. For the establishment of a climatology of the stratospheric-tropospheric exchange it is necessary to have available sufficiently long homogeneous measuring series of all relevant parameters. The measurements of the cosmogenic radionuclides are therefore to be continued.
2. The meteorological analysis of two long-term periods (90 and 60 days resp.) of the tropospheric flow conditions will be concluded. Laws of the tropospheric flow will be established. In this respect it has to be differentiated between days with influx and without influx of stratospheric air.
3. Monitoring of stratospheric aerosol layers will commence. The goal is to determine possible time variations in altitude and thickness of stratospheric aerosol layers.
4. Synchronous recording of the tropospheric ozone at three different altitudes will begin. Parallel to that measurements of other trace gases which might affect the ozone balance are to be conducted. By means of suitable tracers the origin of high ozone concentrations will be investigated. Studies are to be undertaken separately for influx from the stratosphere (tracer Be7) and from areas with photochemical smog (tracer Pb 214, Bi 214). The measurements will be supplemented by measurements

of the total atmospheric ozone.

5. The investigations into the influence of solar events on the stratospheric-tropospheric exchange will be continued.

ABSTRACT

The studies of the stratospheric-tropospheric exchange were continued. The methods described in previous reports were retained.

Continuous data of the cosmogenic nuclides Be7, P32, P33, S35 and of fallout are given for the reporting period.

A lidar system permitting remote sensing of stratospheric aerosol layers is described.

Some examples of application demonstrate the effectiveness of an earlier described method for the forecasting of stratospheric intrusions.

Fresh fallout from a Chinese nuclear weapon test could be identified by means of a GeLi-Gamma-Spectrometer.

A harmonic analysis of the Be7 data resulted in frequencies which suggest a direct influence of solar rotation on the influx of Be7 and thus on the stratospheric-tropospheric exchange.

LEGENDS OF FIGURES

Fig. 1: Block scheme of the lidar system

Fig. 1a: Flow chart of the automatic data accumulation- and storage, to be continued on 1b (intersection A)

Fig. 1b: flow chart of the automatic data processing

Fig. 2: Block scheme, remote control electronics

Fig. 3: Flow chart of the computer program for automatic photon counting measurements

Fig. 4: Rayleigh backscatter returns calculated from radiosonde data

Figs. 5 - 7: Lidar backscatter profile and computed molecular return

Fig. 8: Graphical representation of the concentration of fallout, Be7, P32, P33, S35, ozone, and the amount of precipitation

Fig. 9: Variation of the counting rate of Be7 during the period October through December 1975

Fig. 10: Comparison between measured and prognosticated Be7 -concentration for the same interval of time

Fig. 11: Time variation of the profile of the relative humidity measured with the Munich radiosonde (upper part), and of the relative humidity measured at the station Zugspitze

Fig. 12: Fallout after the Chinese nuclear weapon test of 25 September 1976

12 a: Variation in the Be7-concentration

12 b: Concentration of the fallout in the air

12 c: Schematical representation of the tropospheric flow conditions

12 d: Time variation of the relative humidity profile measured with the Munich radiosonde

12 e: Prognosticated influx intensity of stratospheric air (shaded, values correspond to the standardized Be7-scale) and observed fallout concentration in the air (columns, standardized to maximum value)

Fig. 13: Variation of the total beta-activity in the air during the passage of the fallout cloud

Fig. 14: Gamma spectrum of a precipitation sample taken at Zugspitze, Wank and Garmisch-Partenkirchen (4/5. Oct. 1976)

Fig. 15: Gamma spectrum of an aerosol sample (Zugspitze, 6 October 1976)

Fig. 16: Gamma spectrum of the heavy metal precipitation of aerosol samples (Zugspitze, 6/8. Oct. 1976)

Fig. 17: Gamma spectrum of a high volume aerosol sample (Wank, 6/11. Oct. 1976)

Fig. 18: Smoothed spectrum of the daily Be7-concentration at Zugspitze (2964 m a.s.l.), window N = 471 days, max lag M = 511 days, total period Nov. 1969 - July 1972. The numbers at the frequency peaks indicate the corresponding periods in days

Fig. 19: Smoothed spectrum of the daily relative Be7-concentration at Zugspitze (2964 m a.s.l.), window N = 432 days, max lag M = 511 days, total period July 1972 - January 1975. The numbers at the frequency peaks indicate the corresponding periods in days.

F I G U R E S 1 - 19

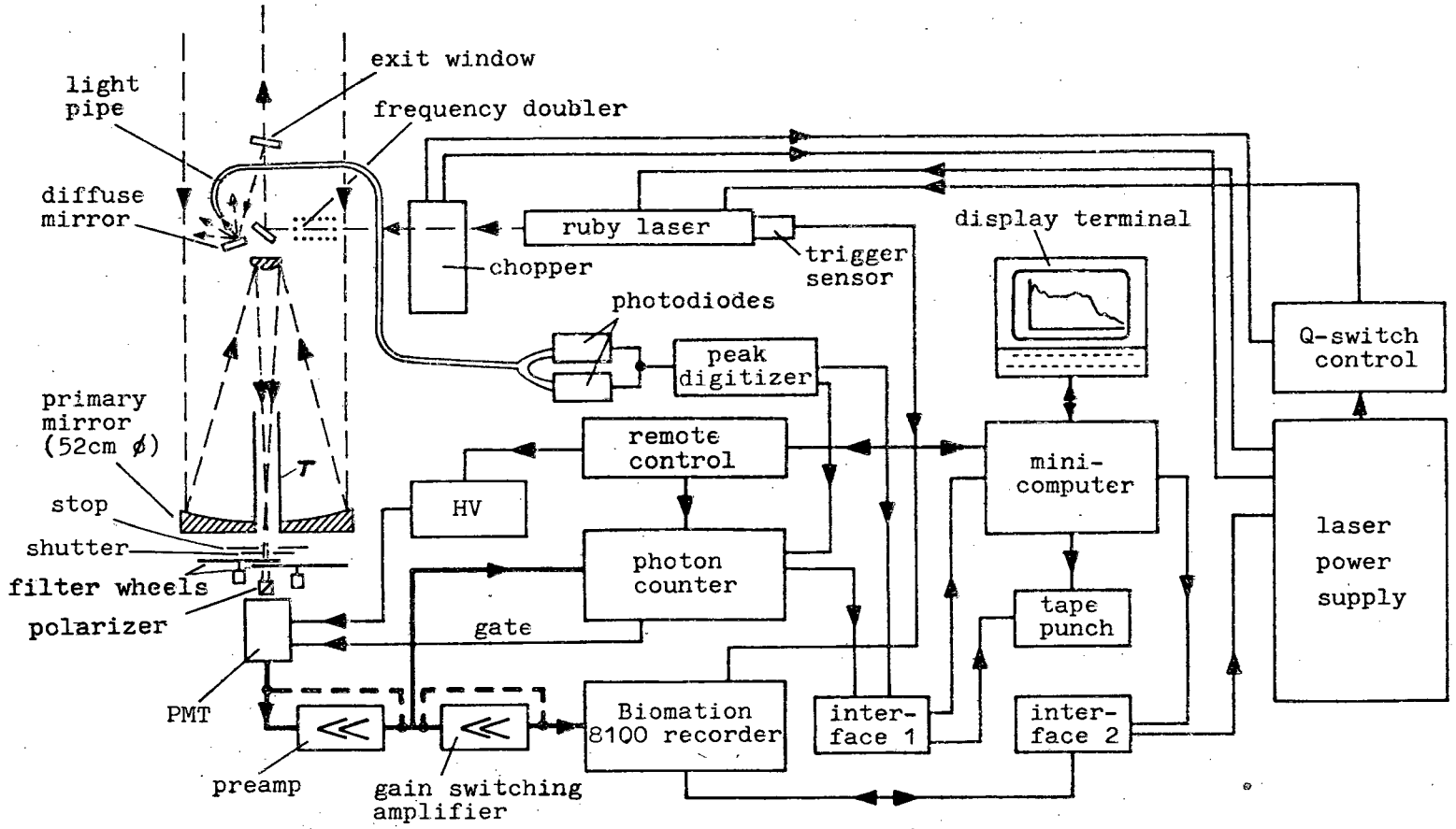
light pipe
exit window
frequency doubler
diffuse mirror
ruby laser
chopper
trigger sensor
display terminal
photodiodes
peak digitizer
Q-switch control
primary mirror (52cm ϕ)
remote control
mini-computer
stop
HV
shutter
photon counter
laser power supply
filter wheels
polarizer
gate
tape punch
PMT
Biomation 8100 recorder
inter-face 1
inter-face 2
preamp
gain switching amplifier

Fig. 1

Fig. 1a

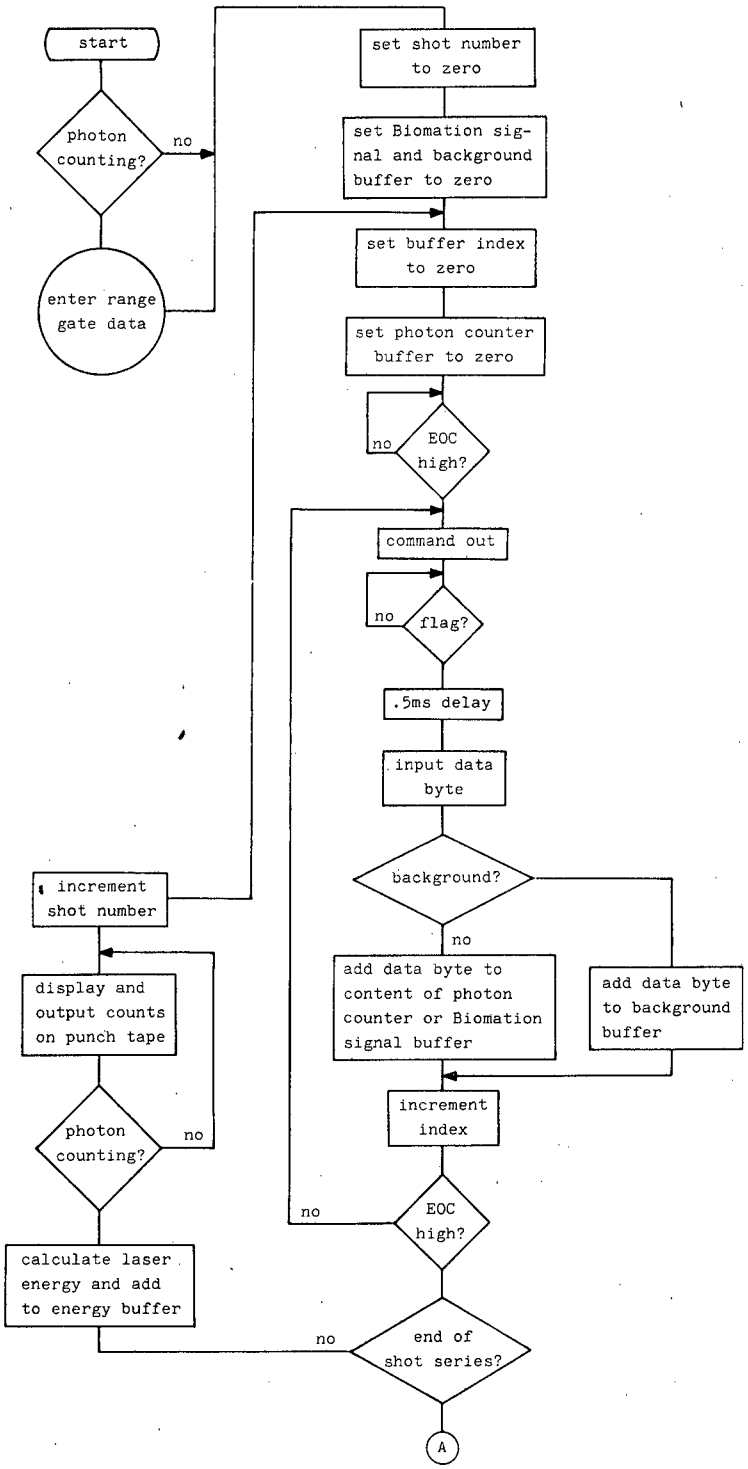
start
photon counting?
no
enter range gate data
set shot number to zero
set Biomation signal and background buffer to zero
set buffer index to zero
set photon counter buffer to zero
no
EOC high?
command out
no
flag?
.5ms delay
input data byte
background?
no
add data byte to content of photon counter or Biomation signal buffer
add data byte to background buffer
increment index
no
EOC high?
increment shot number
display and output counts on punch tape
photon counting?
no
calculate laser energy and add to energy buffer
no
end of shot series?
A

Fig. 1b

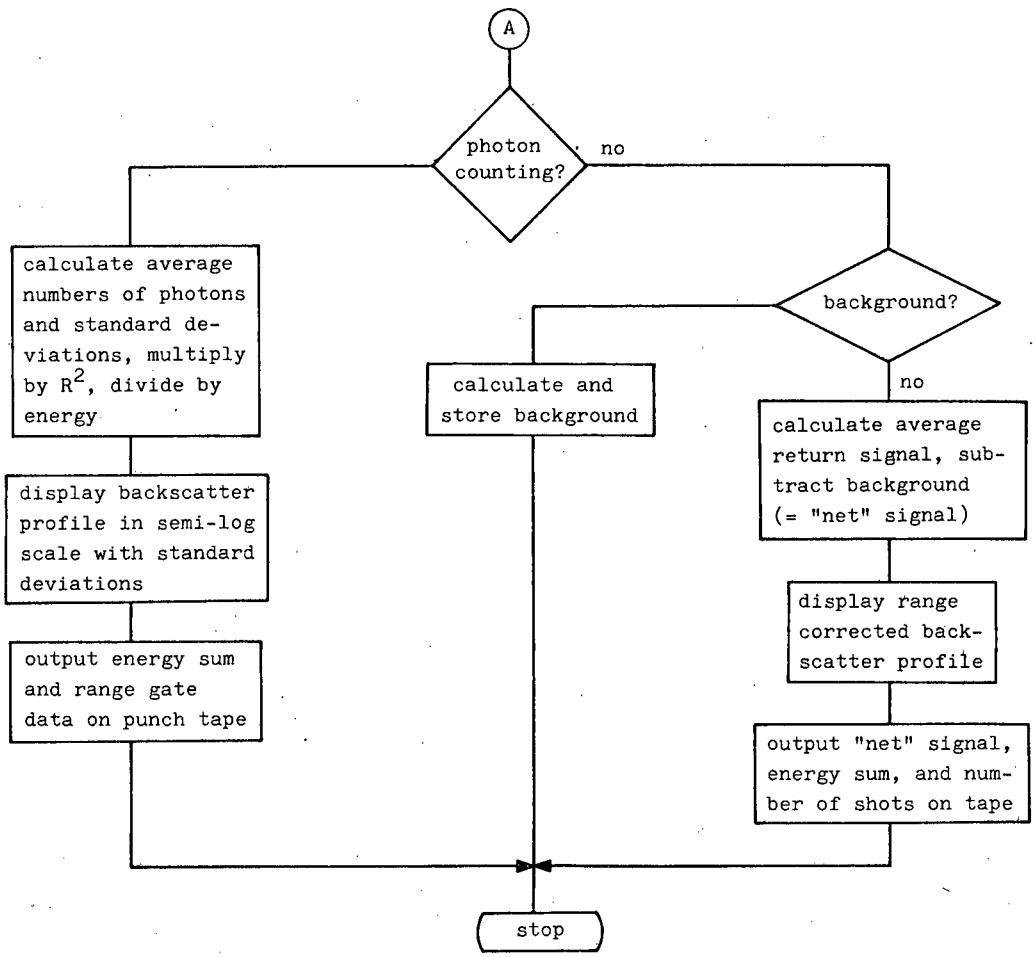
A
photon counting?
no
calculate average numbers of photons and standard deviations, multiply by R^2, divide by energy
display backscatter profile in semi-log scale with standard deviations
output energy sum and range gate data on punch tape
background?
calculate and store background
no
calculate average return signal, subtract background (= "net" signal)
display range corrected backscatter profile
output "net" signal, energy sum, and number of shots on tape
stop

Fig. 2

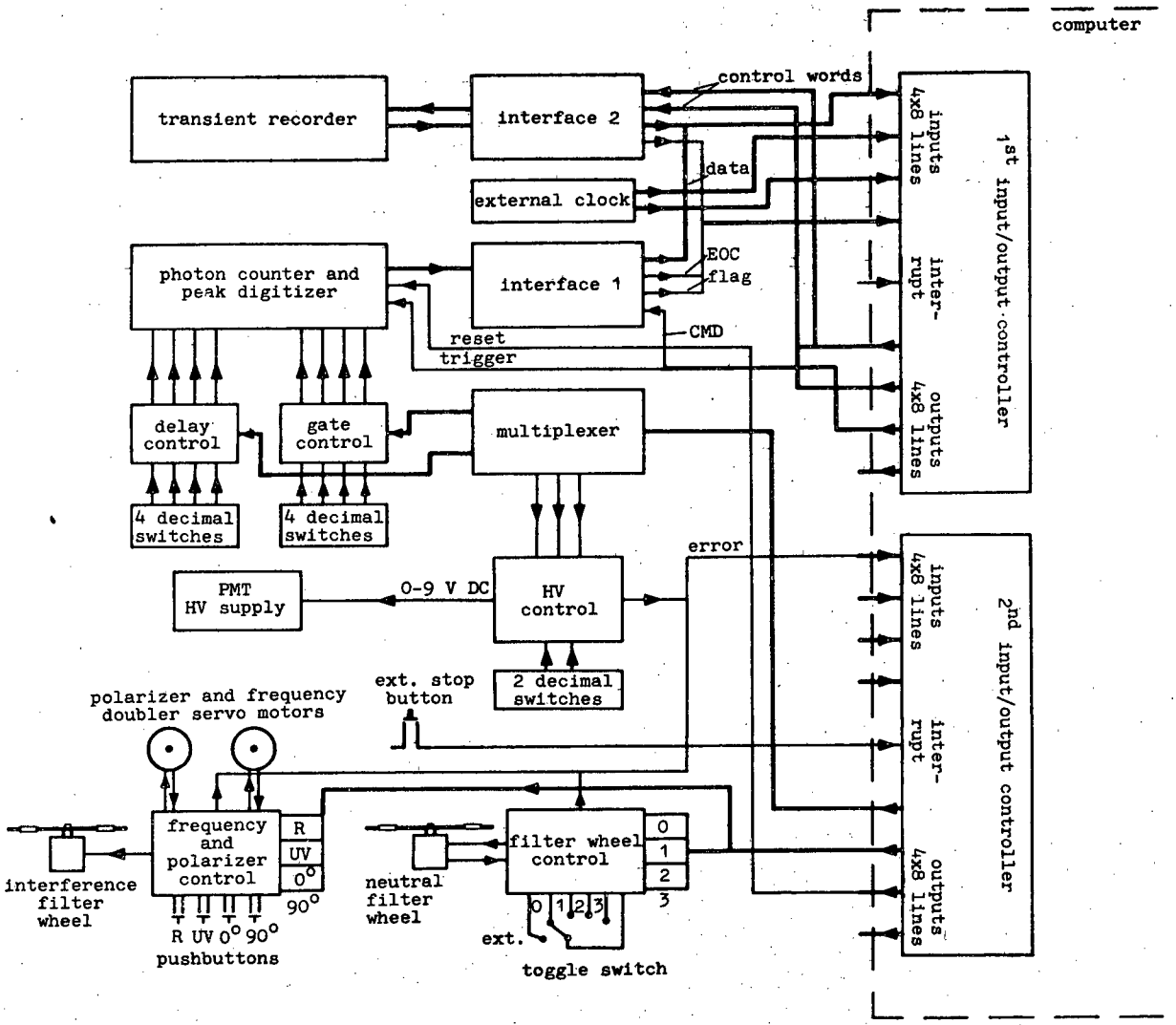
computer
transient recorder
interface 2
control words
data
external clock
photon counter and peak digitizer
interface 1
EOC
flag
CMD
reset
trigger
delay control
gate control
multiplexer
4 decimal switches
4 decimal switches
1st input/output controller
inputs 4x8 lines
inter-rupt
outputs 4x8 lines
error
PMT HV supply
0-9 V DC
HV control
2 decimal switches
2nd input/output controller
ext. stop button
polarizer and frequency doubler servo motors
frequency and polarizer control
R
UV
0°
90°
interference filter wheel
R UV 0° 90°
pushbuttons
neutral filter wheel
filter wheel control
0
1
2
3
ext.
toggle switch

Fig. 3

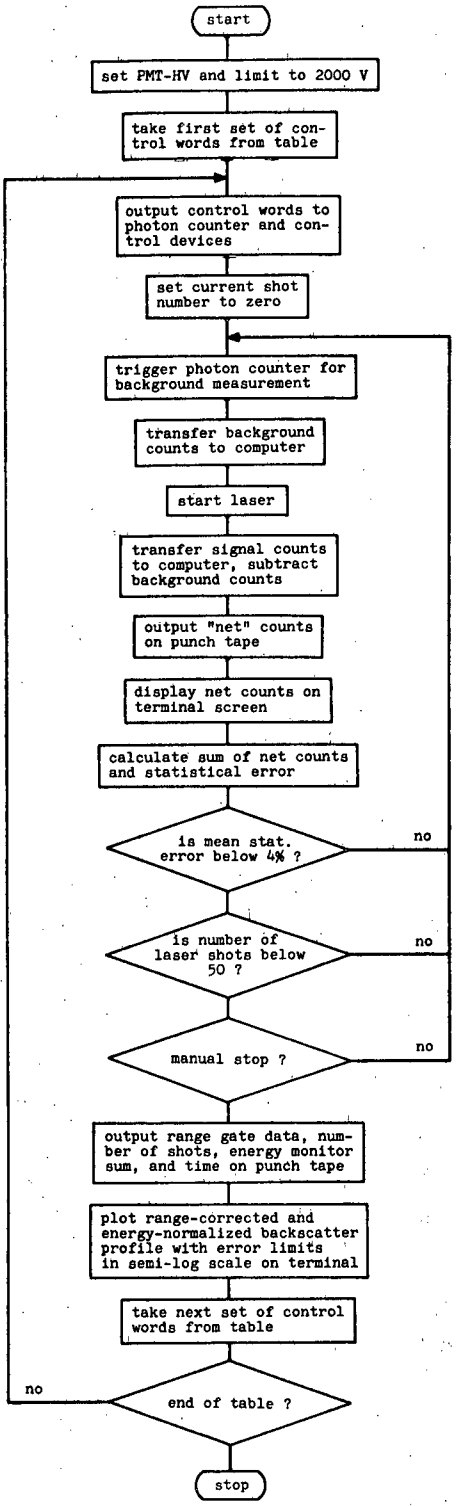
start
set PMT-HV and limit to 2000 V
take first set of control words from table
output control words to photon counter and control devices
set current shot number to zero
trigger photon counter for background measurement
transfer background counts to computer
start laser
transfer signal counts to computer, subtract background counts
output "net" counts on punch tape
display net counts on terminal screen
calculate sum of net counts and statistical error
is mean stat. error below 4% ?
no
is number of laser shots below 50 ?
no
manual stop ?
no
output range gate data, number of shots, energy monitor sum, and time on punch tape
plot range-corrected and energy-normalized backscatter profile with error limits in semi-log scale on terminal
take next set of control words from table
end of table ?
no
stop

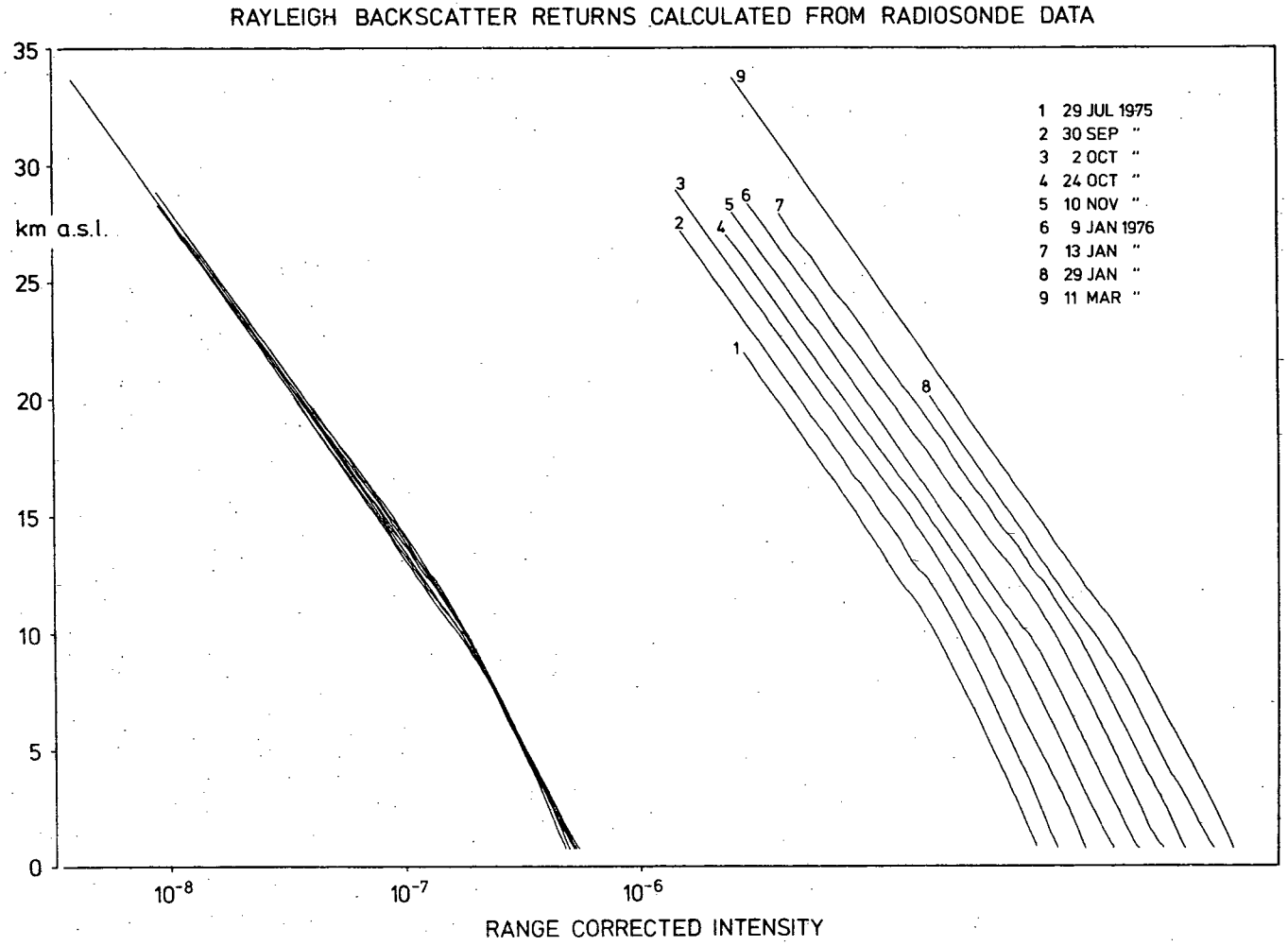
RAYLEIGH BACKSCATTER RETURNS CALCULATED FROM RADIOSONDE DATA
km a.s.l.
35
30
25
20
15
10
5
0
10^{-8}
10^{-7}
10^{-6}
RANGE CORRECTED INTENSITY
1 29 JUL 1975
2 30 SEP "
3 2 OCT "
4 24 OCT "
5 10 NOV "
6 9 JAN 1976
7 13 JAN "
8 29 JAN "
9 11 MAR "

Fig. 4

Fig. 5

LIDAR BACKSCATTER PROFILE AND COMPUTED MOLECULAR RETURN

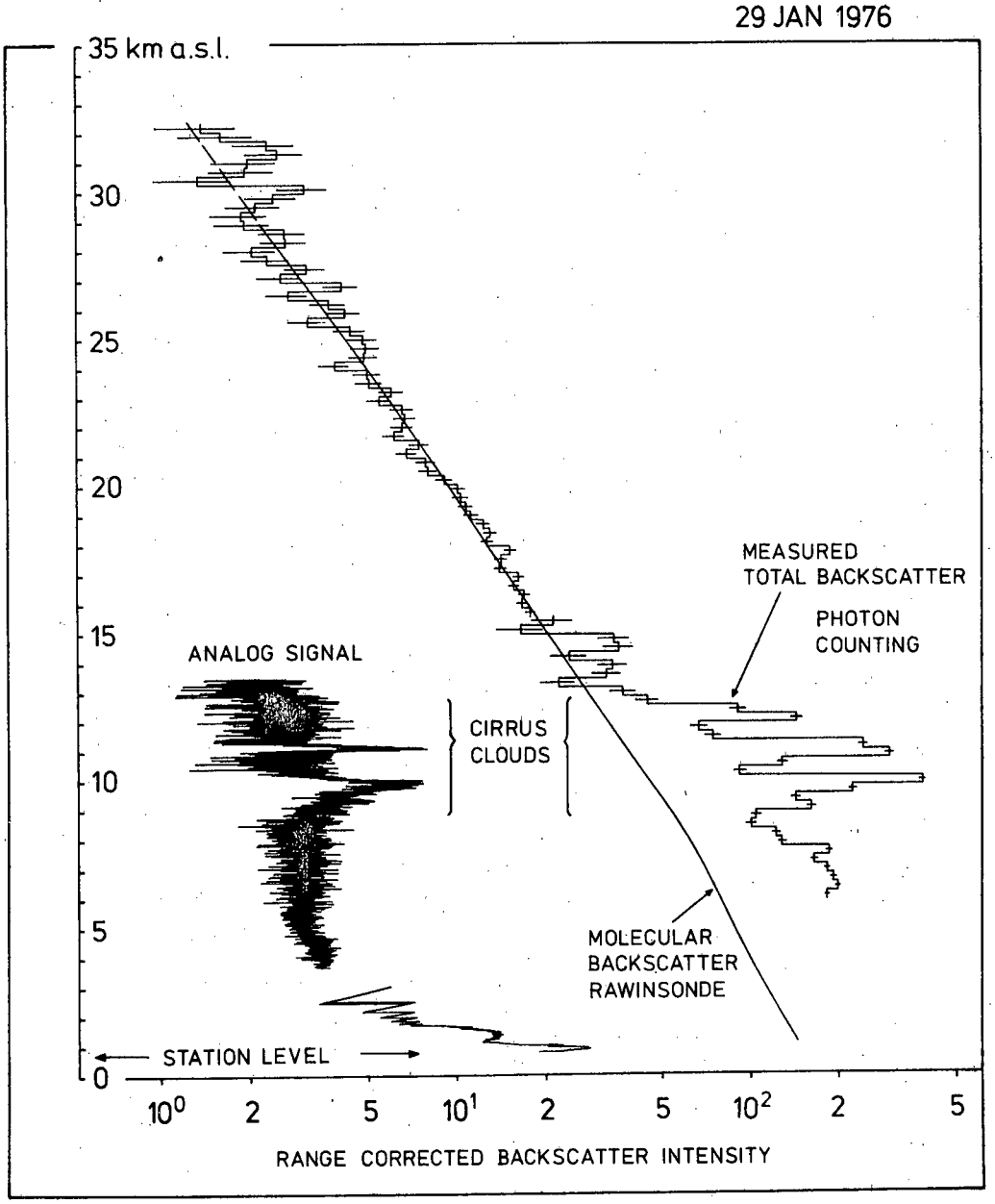

Fig.6

LIDAR BACKSCATTER PROFILE AND COMPUTED MOLECULAR RETURN

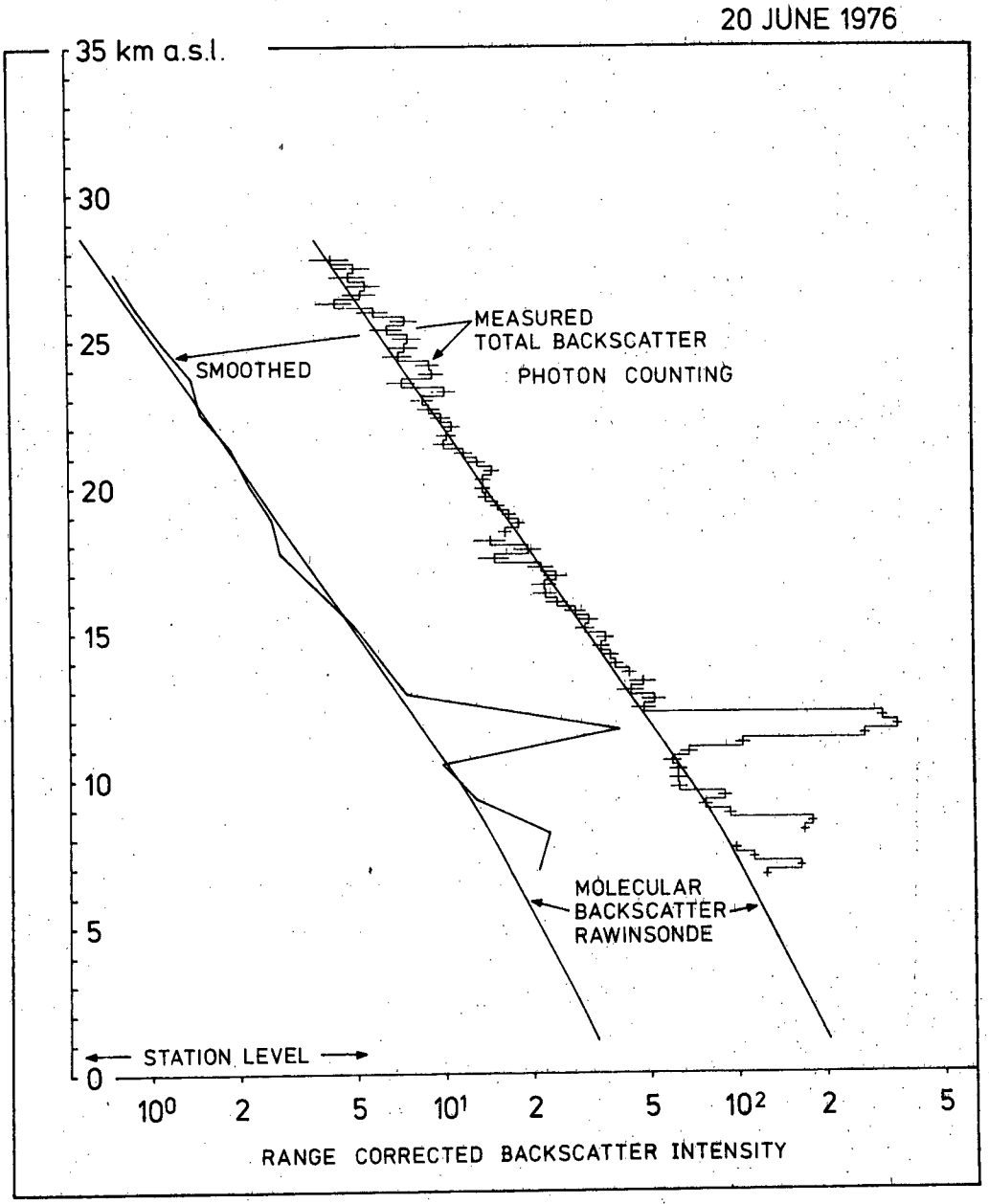

Fig. 7

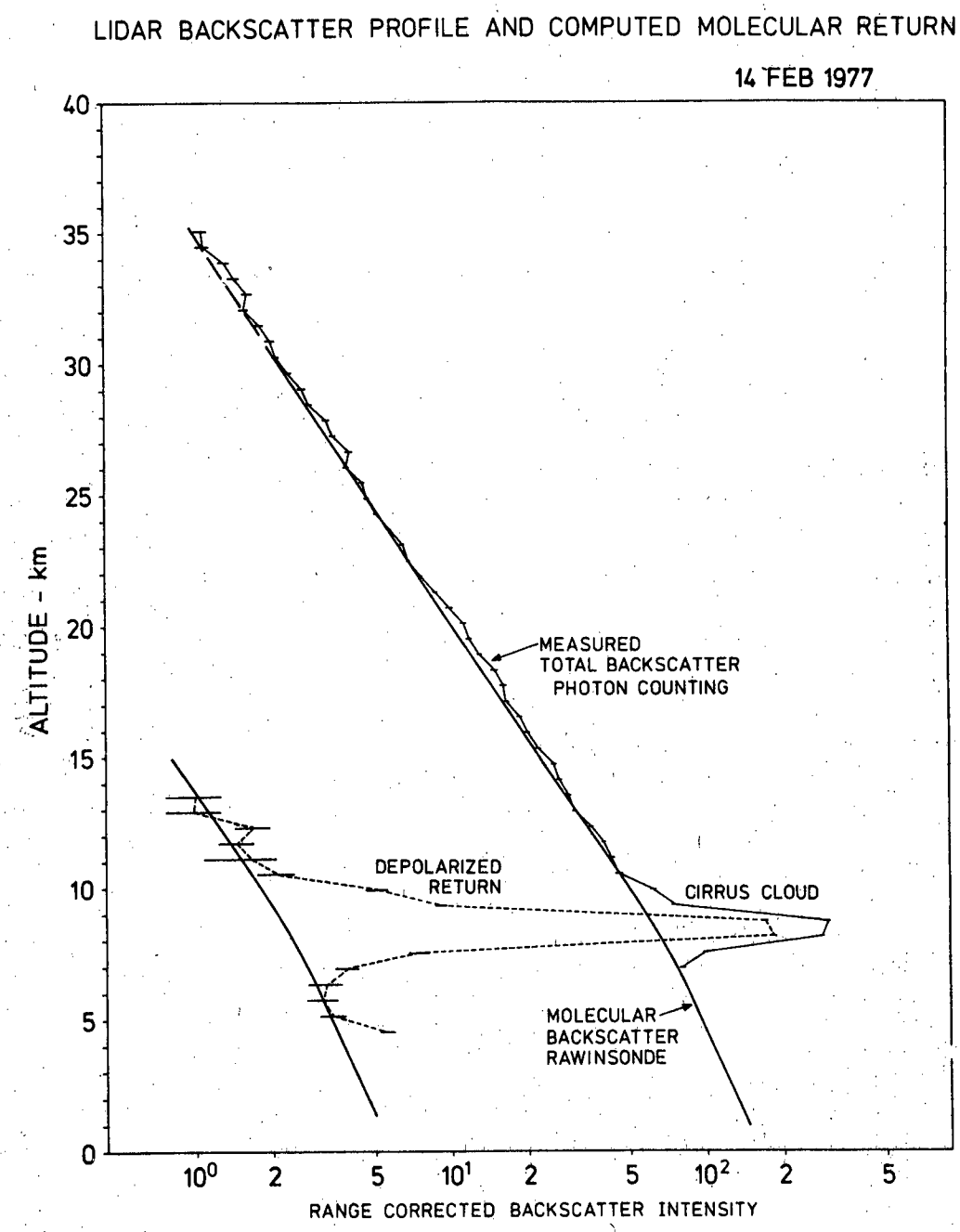
LIDAR BACKSCATTER PROFILE AND COMPUTED MOLECULAR RETURN
14 FEB 1977
ALTITUDE - km
40
35
30
25
20
15
10
5
0
MEASURED
TOTAL BACKSCATTER
PHOTON COUNTING
DEPOLARIZED
RETURN
CIRRUS CLOUD
MOLECULAR
BACKSCATTER
RAWINSONDE
10^0
2
5
10^1
2
5
10^2
2
5
RANGE CORRECTED BACKSCATTER INTENSITY

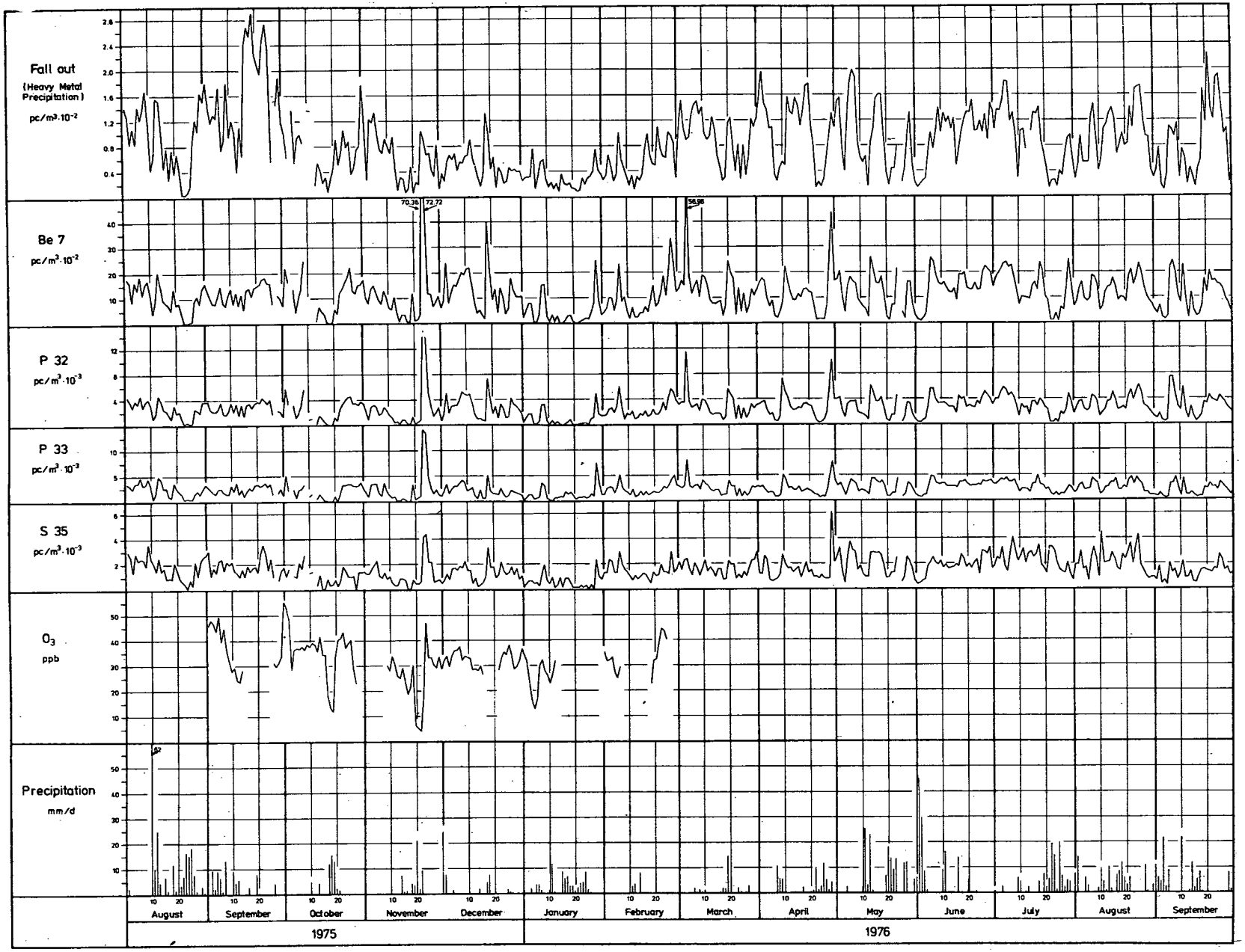
Fall out
(Heavy Metal Precipitation)
pc/m³·10⁻²
Be 7
pc/m³·10⁻²
70,35
72,72
56,98
P 32
pc/m³·10⁻³
P 33
pc/m³·10⁻³
S 35
pc/m³·10⁻³
O₃
ppb
Precipitation
mm/d
August
September
October
November
December
January
February
March
April
May
June
July
August
September
1975
1976

Fig. 8

Fig. 9

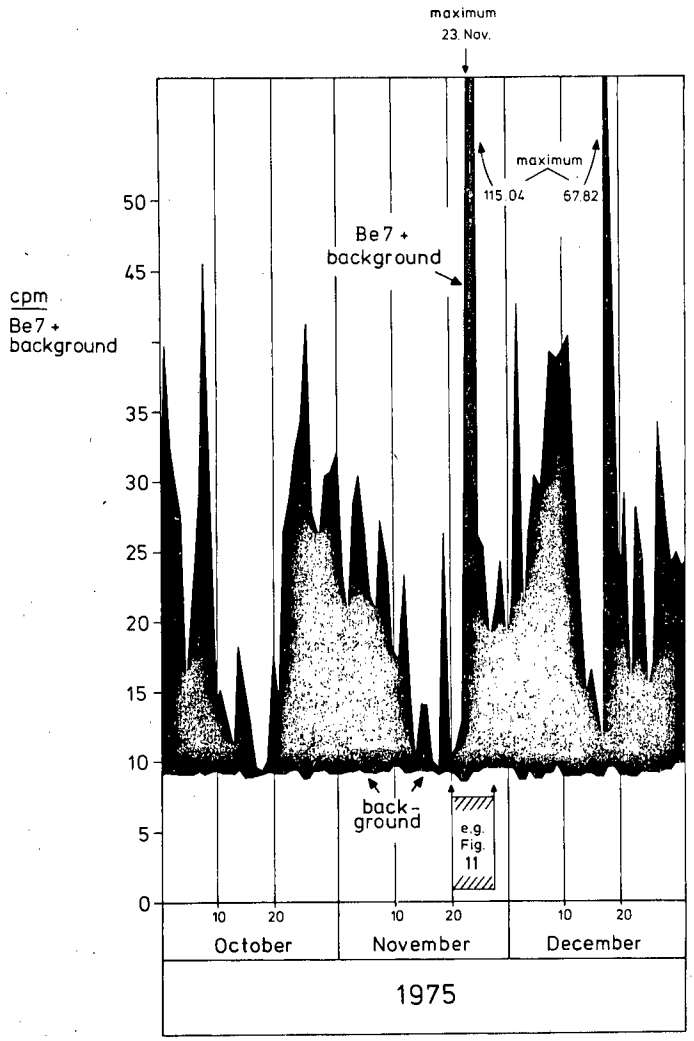
maximum
23. Nov.
maximum
115.04
67.82
Be7 + background
cpm
Be7 + background
50
45
35
30
25
20
15
10
5
0
back-ground
e.g. Fig. 11
10
20
10
20
10
20
October
November
December
1975

Fig. 10

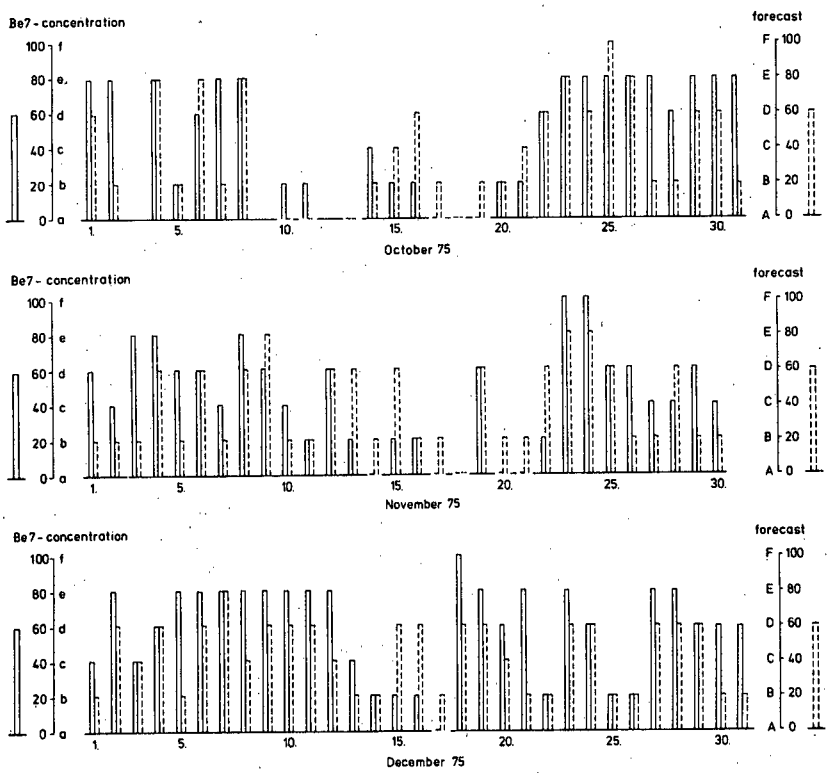
Be7 - concentration
forecast
100 f
80 e
60 d
40 c
20 b
0 a
F 100
E 80
D 60
C 40
B 20
A 0
1. 5. 10. 15. 20. 25. 30.
October 75
Be7 - concentration
forecast
November 75
Be7 - concentration
forecast
December 75

Fig. 11

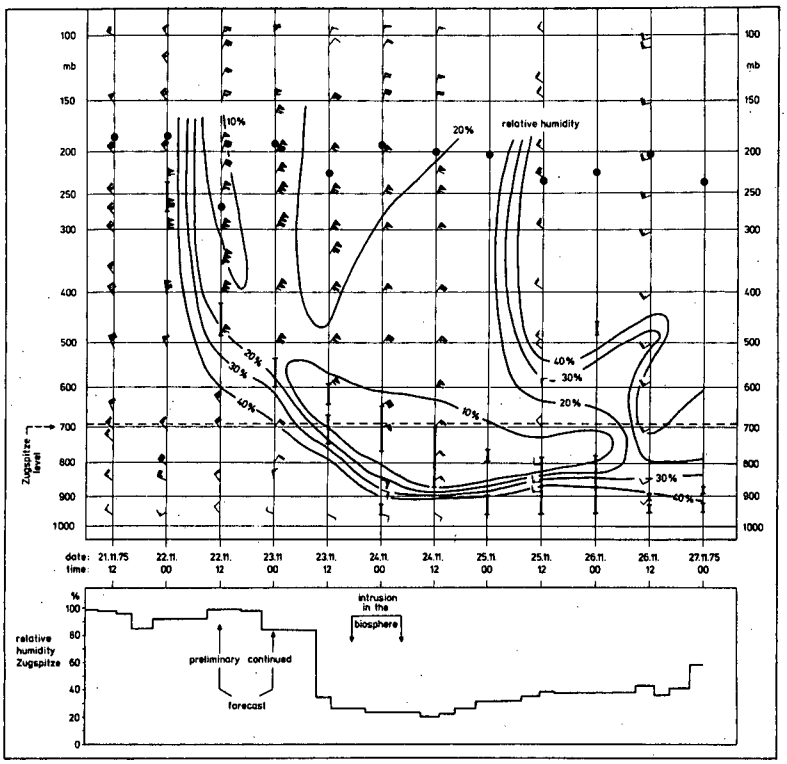
100
mb
150
200
250
300
400
500
600
700
800
900
1000
Zugspitze level
relative humidity
10%
20%
30%
40%
date: 21.11.75 22.11. 22.11. 23.11 23.11. 24.11. 24.11. 25.11. 25.11. 26.11. 26.11. 27.11.75
time: 12 00 12 00 12 00 12 00 12 00 12 00
%
relative humidity Zugspitze
intrusion in the biosphere
preliminary forecast
continued

Fig. 12

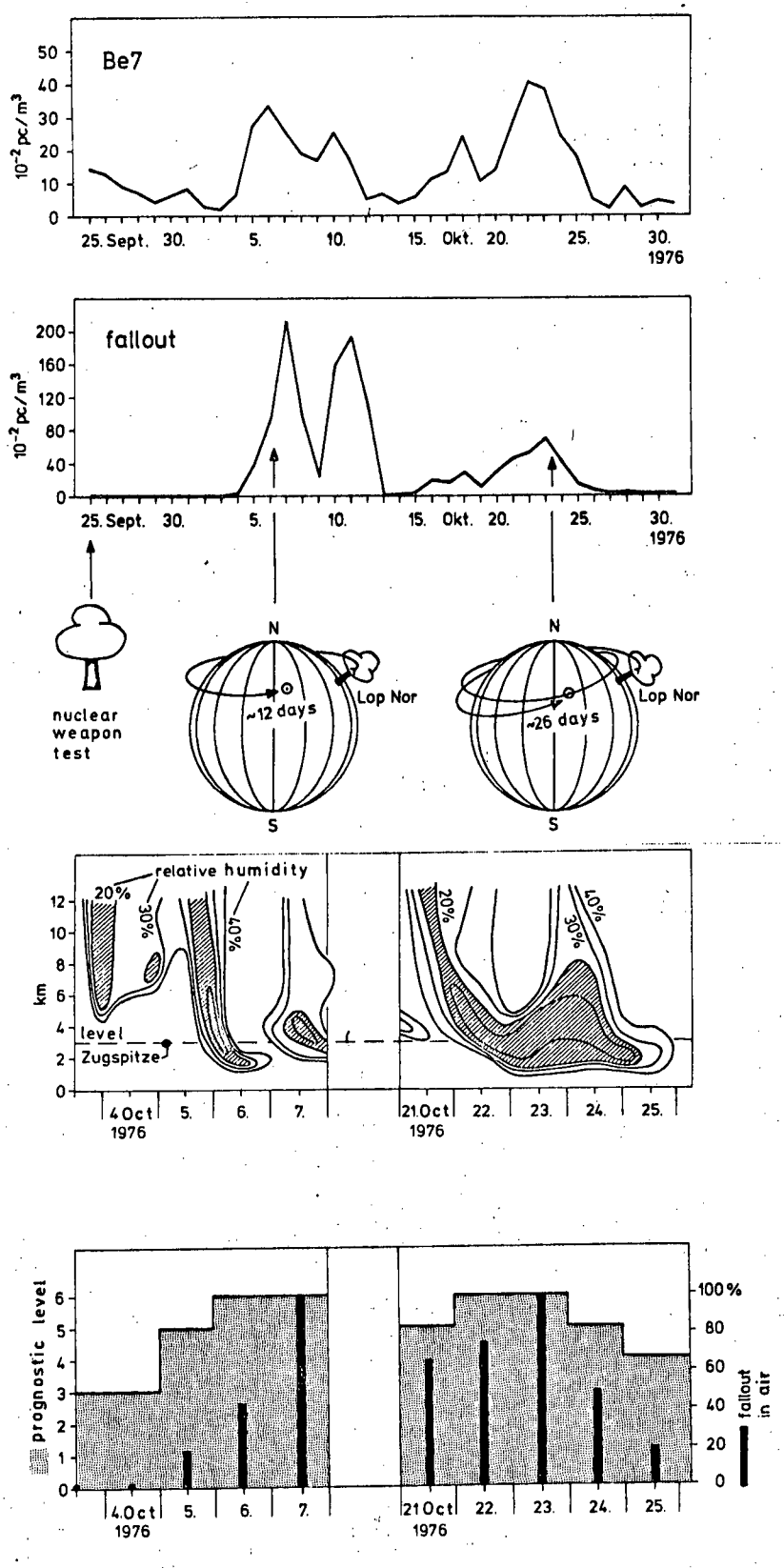
a
Be7
10^{-2} pc/m^3
50
40
30
20
10
0
25. Sept. 30. 5. 10. 15. Okt. 20. 25. 30.
1976
b
fallout
10^{-2} pc/m^3
200
160
120
80
40
0
25. Sept. 30. 5. 10. 15. Okt. 20. 25. 30.
1976
c
nuclear weapon test
N
S
~12 days
Lop Nor
N
S
~26 days
Lop Nor
d
relative humidity
20%
30%
40%
km
12
10
8
6
4
2
0
level
Zugspitze
4 Oct 1976
5.
6.
7.
21 Oct 1976
22.
23.
24.
25.
e
prognostic level
6
5
4
3
2
1
0
100 %
80
60
40
20
0
fallout in air
4 Oct 1976
5.
6.
7.
21 Oct 1976
22.
23.
24.
25.

Fig. 13

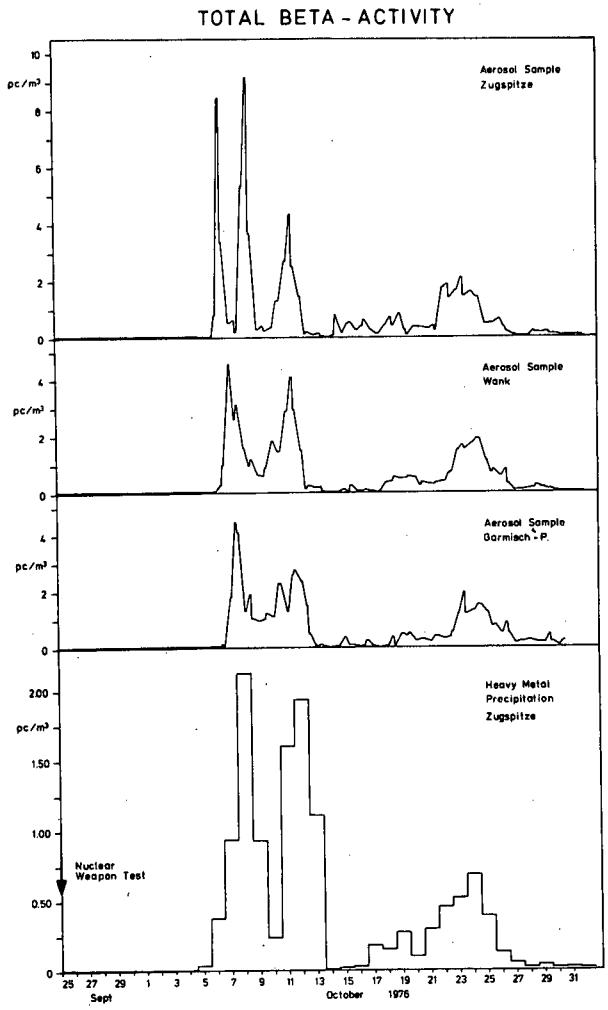
TOTAL BETA - ACTIVITY
Aerosol Sample
Zugspitze
pc/m³
Aerosol Sample
Wank
Aerosol Sample
Garmisch - P.
Heavy Metal
Precipitation
Zugspitze
Nuclear
Weapon Test
Sept
October
1976

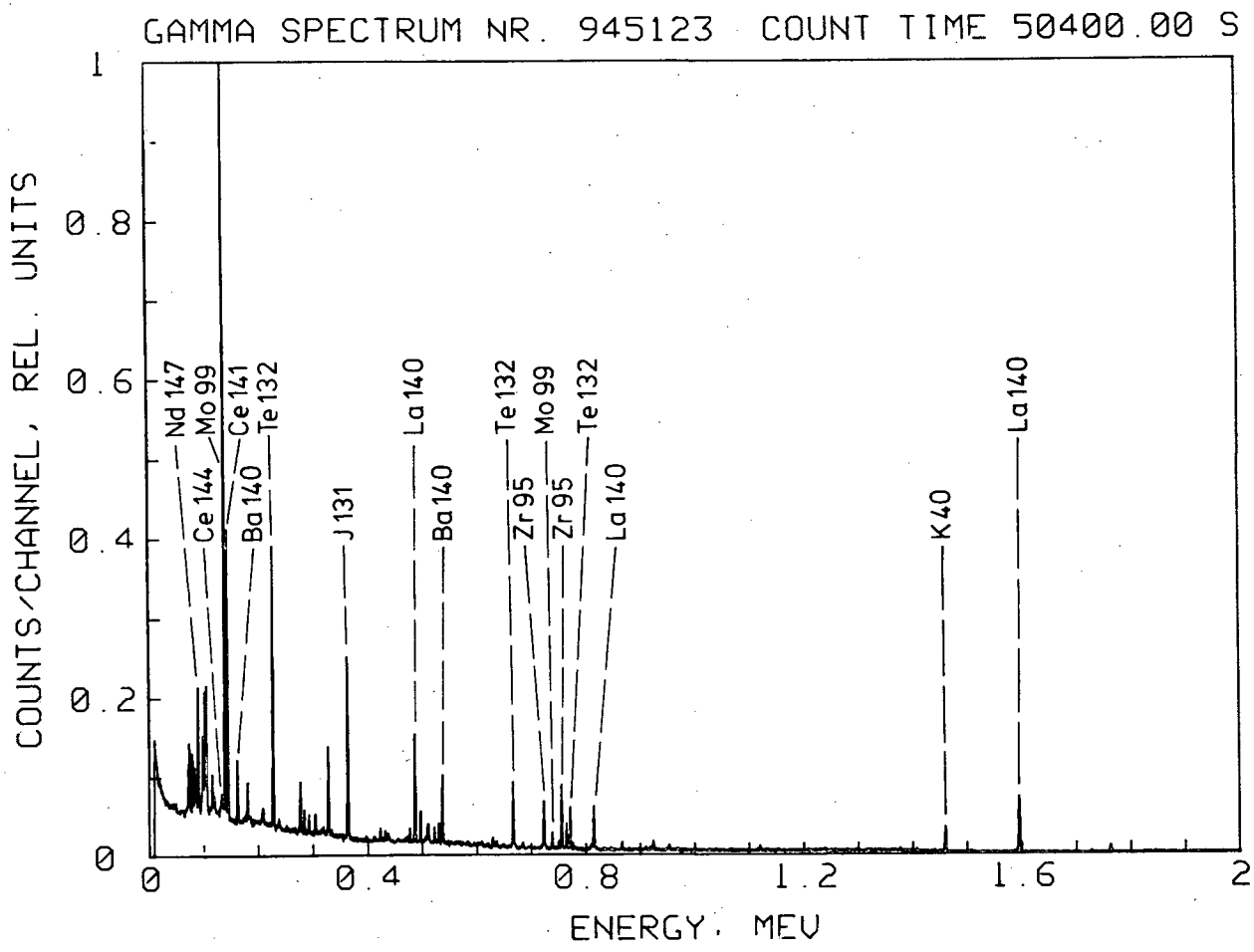

PRECIPITATION ZUGSPITZE, WANK, GARMISCH
4/5 OCT 1976

Fig. 14

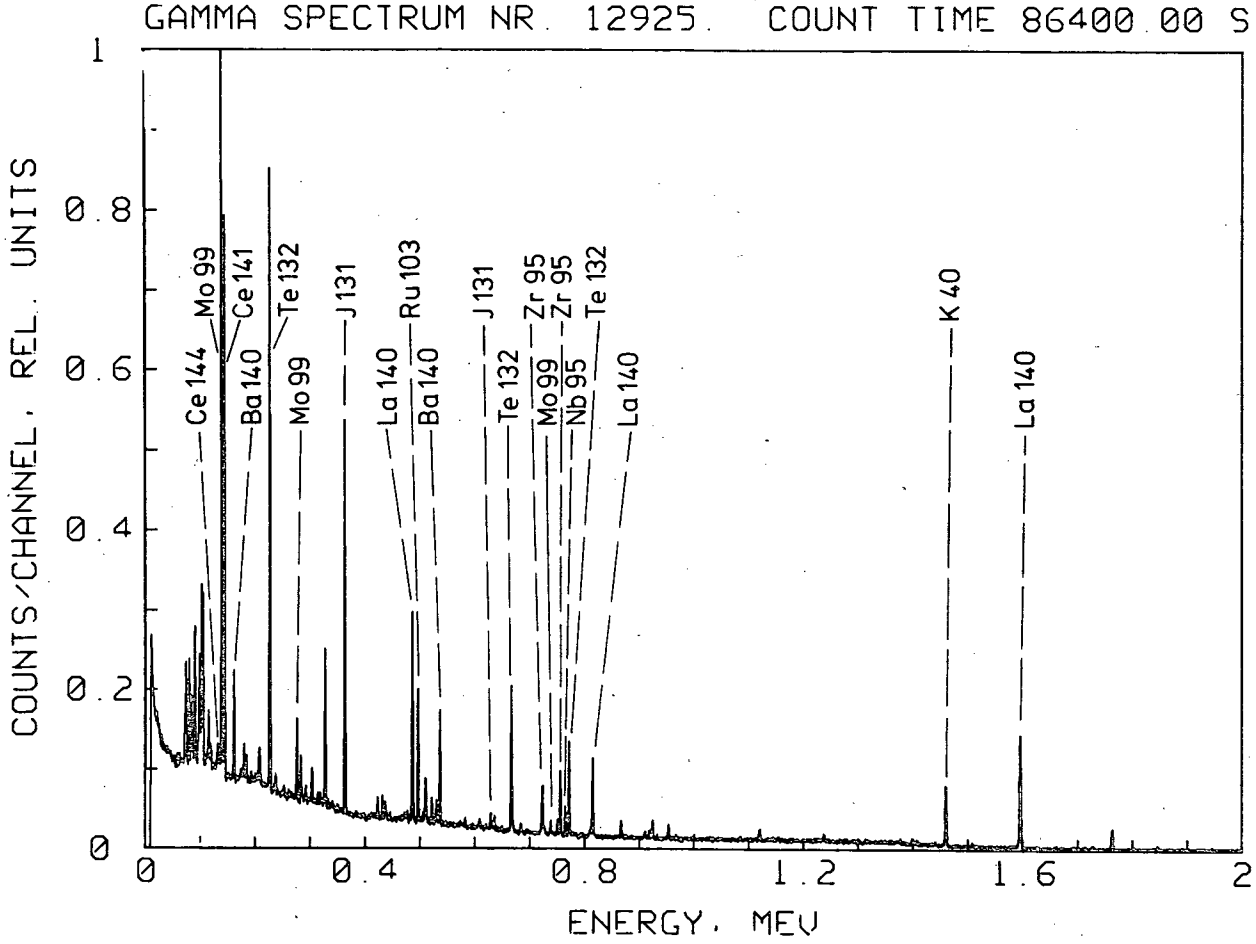

AEROSOL SAMPLE ZUGSPITZE
6 OCT 1976

Fig. 15

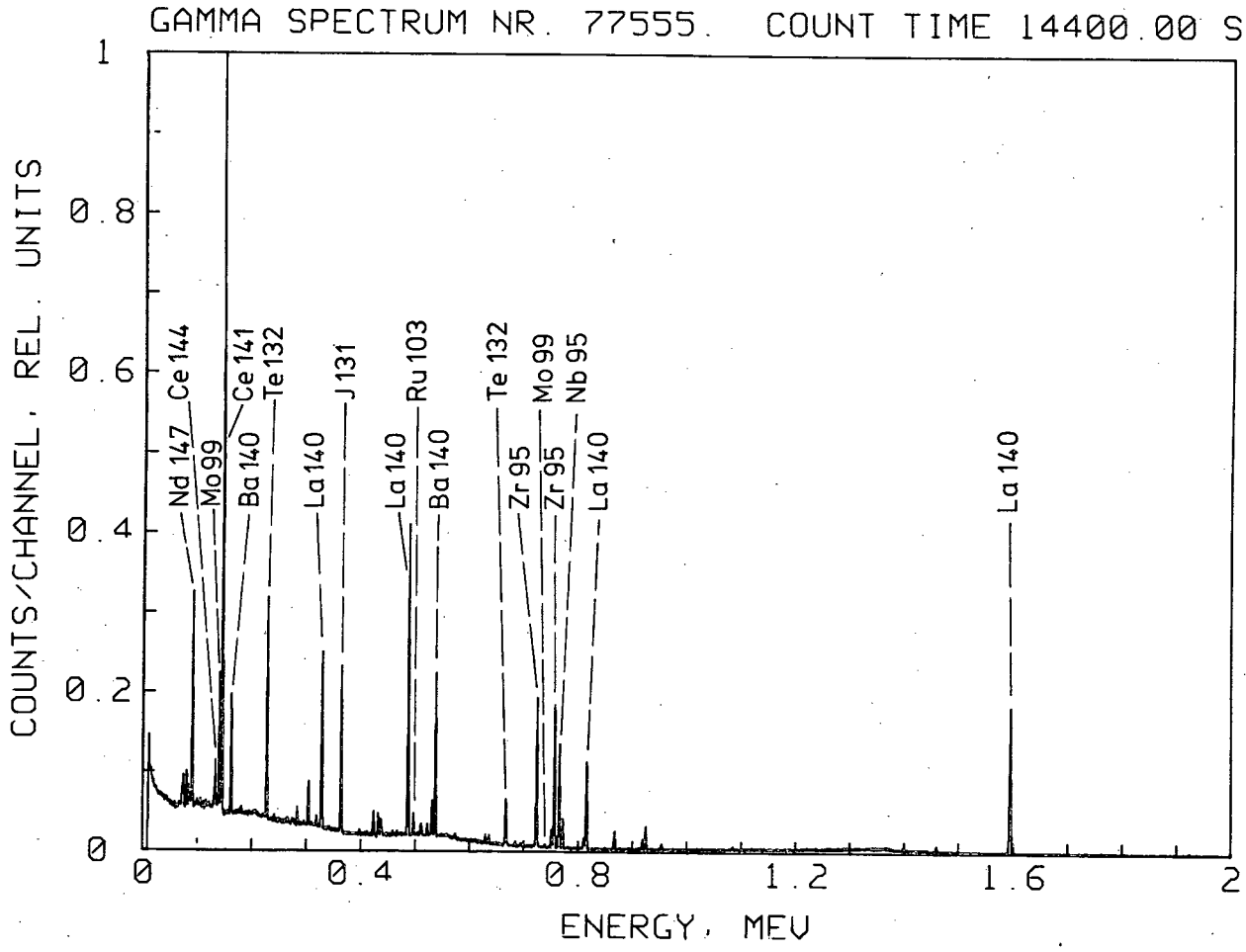

AEROSOL SAMPLE ZUGSPITZE
(HEAVY METAL PREC.) 6-8 OCT 1976

Fig.16

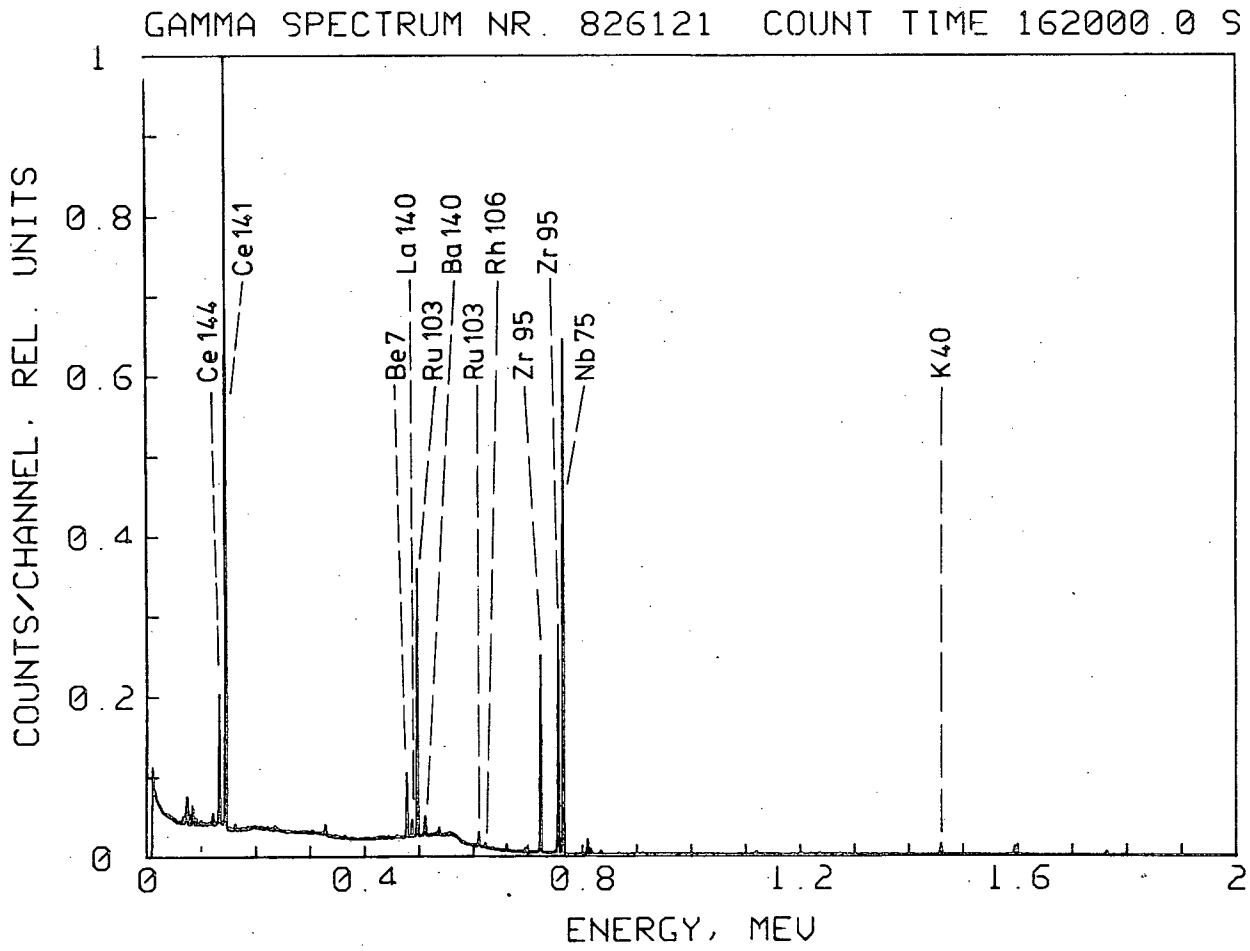

HIGH VOLUME AEROSOL SAMPLE WANK
6 - 11 OCT 1976

Fig. 17

Fig. 18

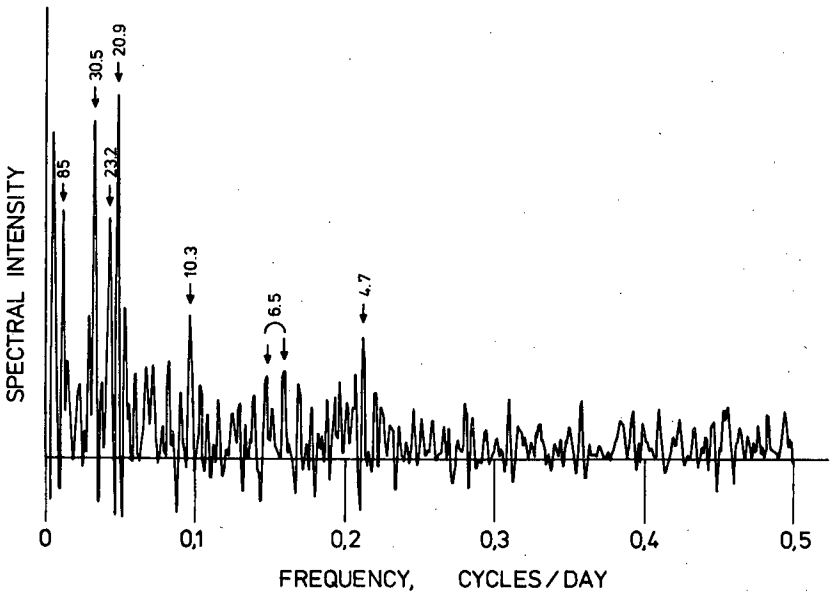
SPECTRAL INTENSITY
85
30.5
20.9
23.2
10.3
6.5
4.7
0
0,1
0,2
0,3
0,4
0,5
FREQUENCY, CYCLES / DAY

Fig. 19

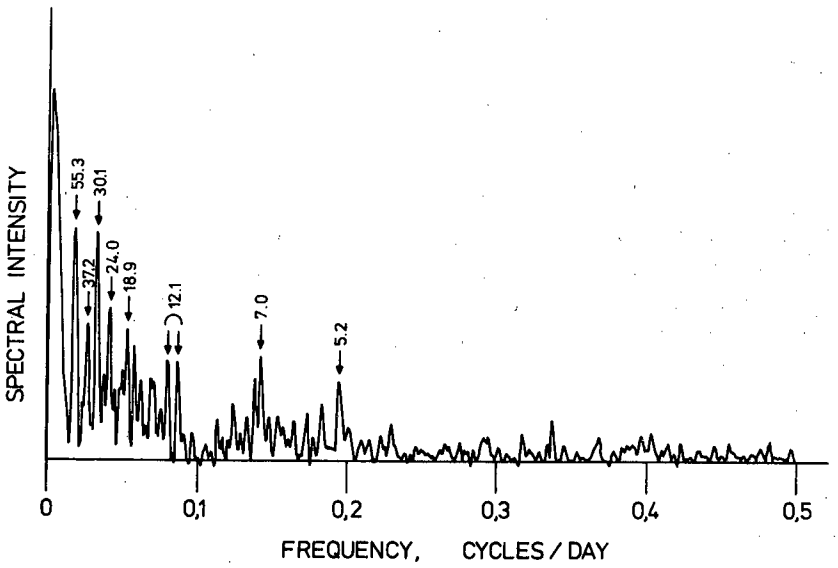
SPECTRAL INTENSITY
55.3
30.1
37.2
24.0
18.9
12.1
7.0
5.2
0
0,1
0,2
0,3
0,4
0,5
FREQUENCY, CYCLES / DAY

A N N E X

RESULTS OF DIURNAL MEASUREMENTS

TABLES I - XIV

Diurnal concentrations of Be7, P32, P33, S35, and some fallout elements (heavy metals) in the air at 2964 m a.s.l. (Zugspitze Peak)

Radioactivity pc/m^3

Aug 1975	fallout $.10^{-2}$	Be7 $.10^{-2}$	P32 $.10^{-3}$	P33 $.10^{-3}$	S35 $.10^{-3}$	03 ppb
1	1.42	17.61	4.42	3.50	2.97	./.
2	1.29	16.27	3.79	3.16	2.59	./.
3	0.86	8.63	2.84	2.52	1.31	./.
4	1.10	16.41	3.92	3.71	2.81	./.
5	0.86	13.38	3.42	3.78	2.28	./.
6	1.43	18.61	4.74	4.86	2.43	./.
7	1.24	11.42	2.85	3.30	2.35	./.
8	1.40	15.46	3.78	3.46	1.85	./.
9	1.69	17.03	4.16	4.63	3.58	./.
10	1.17	11.71	3.26	3.23	2.40	./.
11	0.45	4.04	1.06	0.57	2.03	./.
12	0.65	9.01	1.88	1.81	1.44	./.
13	1.57	20.35	4.71	5.12	2.47	./.
14	1.53	14.82	3.86	4.36	1.43	./.
15	1.08	9,38	2.55	2.68	1.68	./.
16	0.48	8.21	2.34	2.78	0.80	./.
17	0.78	7.20	1.71	1.14	0.89	./.
18	0.30	5.25	1.02	0.85	0.81	./.
19	0.75	13.63	3.15	3.75	2.09	./.
20	0.39	7.46	1.99	2.67	1.53	./.
21	0.69	8.06	2.17	2.05	0.87	./.
22	0.42	4.18	1.09	1.57	0.59	./.
23	0.06	0.38	0.20	0.52	0.39	./.
24	0.05	0.22	0.48	0.68	0.05	./.
25	0.09	0.53	0.27	0.56	0.74	./.
26	0.18	0.76	0.35	0.55	0.28	./.
27	0.84	8.92	2.63	1.68	2.18	./.
28	1.23	10.77	2.37	2.22	1.04	./.
29	1.06	7.90	2.00	1.50	2.22	./.
30	1.65	13.63	3.76	2.47	2.59	./.
31	1.52	15.67	3.77	3.39	2.75	./.

Radioactivity pc/m^3

Sep 1975	fallout $.10^{-2}$	Be7 $.10^{-2}$	P32 $.10^{-3}$	P33 $.10^{-3}$	S35 $.10^{-3}$	03 ppb
1	1.81	12.99	3.81	3.02	3.06	45.59
2	1.43	10.22	2.50	2.42	1.07	47,74
3	1.19	7.92	2.22	1.93	1.69	46.41
4	1.31	7.72	2.23	1.58	1.32	43.49
5	1.26	10.67	2.60	2.56	2.28	49.15
6	1.74	14.60	3.64	2.67	2.42	39.32
7	0.76	8.29	1.86	1.96	1.50	44.44
8	0.92	7.00	1.71	1.63	2.21	36.26
9	1.81	11.29	2.36	1.55	1.98	31.73
10	0.97	13.74	3.62	3.27	2.19	27.58
11	1.22	7.85	2.18	2.18	1.49	29.04
12	1.04	12.19	3.47	3.85	1.30	24.04
13	0.42	7.26	1.64	1.61	1.00	23.4
14	1.12	11.41	3.27	2.54	1.60	27.97
15	0.67	5.62	1.51	1.15	1.02	./.
16	2.41	13.30	3.36	2.21	1.88	./.
17	2.69	13.97	3.54	2.88	1.44	./.
18	2.55	10.82	2.81	2.37	1.70	./.
19	2.92	14.15	3.49	3.35	1.84	./.
20	2.25	14.81	3.79	3.56	1.37	./.
21	2.09	15.52	3.66	3.18	2.83	./.
22	1.96	17.53	4.42	3.38	3.56	./.
23	2.49	18.12	3.96	3.83	2.89	./.
24	2.74	15.97	3.49	3.06	1.56	./.
25	2.37	15.79	4.14	3.66	2.46	./.
26	0.58	7.85	1.84	1.59	1.01	30.77
27	./.	./.	./.	./.	./.	29.59
28	1.46	11.08	2.34	1.85	0.74	31.02
29	1.89	9.74	2.21	2.70	1.45	33.51
30	1.17	7.19	1.45	1.36	1.76	54.85

Radioactivity pc/m^3

Okt 1975	fallout $.10^{-2}$	Be7 $.10^{-2}$	P32 $.10^{-3}$	P33 $.10^{-3}$	S35 $.10^{-3}$	03 ppb
1	1.00	21.79	5.84	5.29	1.03	52.81
2	0.64	16.42	3.44	2.33	1.64	48.60
3	./.	./.	./.	./.	./.	28.35
4	1.38	13.44	3.21	2.46	1.09	36.19
5	0.56	4.46	1.27	0.90	0.97	36.73
6	0.94	9.43	1.95	2.44	2.14	36.47
7	1.00	13.33	3.18	2.67	1.68	37.43
8	0.87	24.69	5.76	3.42	2.75	36.15
9	./.	./.	./.	./.	./.	38.32
10	1.38	3.65	0.98	1.16	1.33	37.39
11	1.37	4.18	1.12	1.64	1.41	38.91
12	./.	./.	./.	./.	./.	38.23
13	0.21	0.98	0.35	0.69	0.34	35.56
14	0.55	6.44	1.58	1.55	1.15	41.37
15	0.43	4.71	1.17	0.95	0.03	34.19
16	0.24	3.60	0.61	0.29	0.08	34.24
17	0.33	0.22	0.18	0.18	0.82	17.78
18	0.10	0.00	0.00	0.00	0.32	13.24
19	0.31	0.46	0.13	0.17	0.41	11.80
20	0.47	5.51	1.30	1.17	0.75	33.85
21	0.92	3.89	0.78	0.15	0.26	40.02
22	0.53	12.05	2.62	1.62	0.73	40.72
23	0.71	13.73	3.40	3.34	1.82	43.03
24	1.07	16.20	3.98	3.36	1.49	36.88
25	0.80	18.29	4.52	3.58	1.02	38.68
26	0.89	22.0	4.63	3.57	0.98	39.94
27	0.38	12.86	3.49	3.20	1.07	28.50
28	0.47	11.92	3.52	3.13	0.00	22.98
29	0.76	15.09	3.23	3.28	1.36	./.
30	0.82	15.33	3.79	3.86	1.36	./.
31	1.77	17.02	3.48	2.66	1.41	./.

Radioactivity pc/m^3

Nov 1975	fallout $.10^{-2}$	Be7 $.10^{-2}$	P32 $.10^{-3}$	P33 $.10^{-3}$	S35 $.10^{-3}$	O3 ppb
1	1.17	10.04	2.32	1.88	1.25	./.
2	0.29	7.90	0.94	1.00	1.26	./.
3	1.24	13.48	2.97	3.51	1.65	./.
4	1.19	14.90	3.27	3.63	1.96	./.
5	1.34	12.04	2.94	3.60	2.29	./.
6	1.01	9.21	1.74	1.80	1.08	./.
7	0.76	7.71	1.93	1.20	0.93	./.
8	0.71	12.85	2.91	3.77	1.35	./.
9	0.93	10.17	2.43	2.19	0.84	29.77
10	0.82	6.08	1.64	1.35	1.05	27.96
11	0.71	5.37	1.32	0.89	0.52	33.62
12	0.96	10.28	0.49	1.05	0.32	30.39
13	0.45	4.45	0.59	0.23	0.32	25.78
14	0.13	0.64	0.25	0.23	0.85	24.91
15	0.32	3.36	0.89	0.72	0.83	28.99
16	0.30	3.32	0.83	0.49	0.72	23.63
17	0.09	0.51	0.27	0.09	0.04	18.71
18	0.14	0.40	0.16	0.10	0.01	21.18
19	0.49	11.78	1.36	3.43	0.75	29.99
20	0.08	0.97	0.19	0.44	0.46	6.38
21	0.24	1.37	0.53	0.85	0.44	5.21
22	0.21	3.37	0.85	1.15	0.64	4.18
23	1.05	70.36	15.43	14.30	4.18	16.82
24	0.90	72.72	13.89	13.59	4.44	46.75
25	0.68	11.63	5.23	4.87	2.17	32.97
26	0.70	11.32	3.01	2.60	2.16	32.90
27	0.44	6.64	1.47	1.64	0.58	30.13
28	0.34	8.27	2.08	2.43	0.67	29.01
29	0.83	10.64	2.86	1.47	0.78	33.26
30	0.15	6.21	0.80	1.14	0.48	28.69

Radioactivity pc/m^3

Dez 1975	fallout $.10^{-2}$	Be7 $.10^{-2}$	P32 $.10^{-3}$	P33 $.10^{-3}$	S35 $.10^{-3}$	03 ppb
1	0.38	8.68	1.86	2.17	0.75	31.95
2	0.26	23.62	5.12	3.54	1.23	33.59
3	0.57	7.98	1.99	1.66	0.77	29.60
4	0.67	11.88	3.08	2.55	1.64	33.69
5	0.60	15.03	3.18	3.13	1.70	35.77
6	0.69	14.57	3.19	3.15	1.53	35.91
7	0.43	17.27	3.98	3.68	1.83	37.28
8	0.56	19.93	5.35	4.33	1.71	31.93
9	0.54	19.05	4.98	3.90	2.25	33.53
10	0.65	21.39	4.79	2.19	1.52	33.03
11	0.67	21.81	5.01	2.49	1.53	32.61
12	0.91	15.02	3.51	2.84	0.46	28.26
13	0.61	8.35	1.76	1.18	0.89	28.56
14	0.48	3.90	1.05	0.62	0.22	27.87
15	0.31	4.98	1.10	2.39	0.37	29.67
16	0.18	3.16	0.80	0.68	0.56	26.39
17	0.34	1.55	0.67	0.73	1.01	./.
18	1.32	39.69	7.39	5.28	3.33	./.
19	1.02	20.22	4.26	2.16	1.74	./.
20	0.45	9.15	1.87	1.65	1.79	./.
21	0.63	13.23	3.00	1.56	0.91	./.
22	0.16	4.18	1.14	1.36	1.17	28.17
23	0.47	13.73	3.36	2.67	2.18	32.34
24	0.39	10.25	2.65	1.53	1.46	35.10
25	0.22	3.59	1.20	0.87	1.17	33.99
26	0.25	5.51	1.34	1.23	1.34	37.86
27	0.47	17.55	4.30	2.30	1.78	34.03
28	0.42	12.98	3.34	1.95	1.15	28.38
29	0.44	10.35	2.99	1.71	1.64	29.53
30	0.40	10.34	2.50	1.52	0.79	31.64
31	0.41	10.41	1.82	1.25	1.07	36.42

Radioactivity pc/m^3

Jan 1976	fallout $.10^{-2}$	Be7 $.10^{-2}$	P32 $.10^{-3}$	P33 $.10^{-3}$	S35 $.10^{-3}$	O3 ppb
1	0.25	2.63	0.58	0.18	0.18	34.43
2	0.30	5.11	1.26	0.77	0.47	32.03
3	0.31	8.03	1.92	1.42	0.70	23.98
4	0.31	8.03	1.92	1.42	0.70	16.38
5	0.75	0.62	0.28	0.50	0.47	12.92
6	0.13	0.49	0.27	0.71	0.55	16.93
7	0.32	3.55	0.68	0.94	0.27	30.05
8	0.55	15.13	3.33	3.73	1.19	32.23
9	0.58	15.51	3.39	3.19	1.98	27.89
10	0.27	2.91	0.83	0.61	0.71	26.18
11	0.15	0.80	0.17	0.30	0.45	23.12
12	0.22	3.51	0.85	0.11	0.95	26.83
13	0.12	0.80	0.27	0.76	0.13	31.83
14	0.20	3.11	0.64	0.80	0.34	./.
15	0.08	0.14	0.23	1.01	0.93	./.
16	0.35	0.14	0.05	0.82	0.17	./.
17	0.20	1.33	0.30	1.94	0.87	./.
18	0.18	3.11	0.61	1.47	0.90	./.
19	0.21	3.36	0.98	1.85	0.53	./.
20	0.13	1.03	0.19	1.22	0.13	./.
21	0.12	0.12	0.15	0.40	0.15	./.
22	0.08	0.42	0.23	0.80	0.11	./.
23	0.10	1.01	0.36	0.75	0.32	./.
24	0.29	1.64	0.41	0.97	0.13	./.
25	0.19	2.17	0.42	0.65	0.31	./.
26	0.29	1.89	0.16	0.84	0.00	./.
27	0.32	4.25	1.10	1.50	0.36	./.
28	0.39	7.59	1.33	0.98	0.00	./.
29	0.74	24.83	5.09	7.60	2.35	./.
30	0.42	9.10	1.87	3.78	1.04	./.
31	0.35	3.62	1.59	1.30	0.79	33.84

VII

Radioactivity pc/m^3

Feb 1976	fallout $.10^{-2}$	Be7 $.10^{-2}$	P32 $.10^{-3}$	P33 $,10^{-3}$	S35 $.10^{-3}$	03 ppb
1	0.26	4.52	1.59	1.40	1.32	35.14
2	0.33	5.96	1.80	2.54	1.30	31.74
3	0.65	10.06	2.59	2.83	2.36	32.23
4	0.47	9.96	2.82	2.70	2.23	33.24
5	0.24	5.01	2.01	1.62	1.32	27.23
6	0.34	9.54	3.09	2.89	1.35	24.99
7	1.00	23.34	6.17	5.30	3.00	29.21
8	0.57	8.73	3.00	2.69	2.02	./.
9	0.44	10.35	1.00	1.99	1.56	./.
10	0.31	5.15	1.94	1.74	1.33	./.
11	0.17	2.03	1.64	1.18	1.02	./.
12	0.33	6.31	2.27	2.35	0.68	./.
13	0.11	2.60	1.05	0.80	1.05	./.
14	0.31	2.54	1.22	1.16	0.79	./.
15	0.25	4.24	1.87	1.93	0.98	./.
16	0.35	4.37	1.59	1.12	1.24	./.
17	0.74	6.62	2.29	1.89	1.14	./.
18	0.98	4.73	1.42	1.17	0.80	./.
19	0.65	9.14	1.68	1.56	0.45	22.91
20	0.51	14.88	2.48	1.88	1.32	31.91
21	0.49	6.87	1.74	1.67	1.06	32.51
22	1.09	7.99	1.74	1.73	1.12	38.61
23	0.75	12.10	2.43	2.11	1.95	44.34
24	0.63	18.61	3.62	2.89	1.34	43.58
25	0.61	11.13	2.39	2.48	1.33	40.21
26	1.01	19.95	4.49	3.23	1.20	./.
27	0.96	33.38	5.80	4.36	2.96	./.
28	0.85	23.31	5.16	5.13	1.31	./.
29	0.30	12.68	3.88	3.13	1.58	./.

Radioactivity pc/m^3

März 1976	fallout $.10^{-2}$	Be7 $.10^{-2}$	P32 $.10^{-3}$	P33 $.10^{-3}$	S35 $.10^{-3}$	O3 ppb
1	1.09	13.77	3.29	2.82	2.17	./.
2	1.50	16.85	3.68	2.53	1.54	./.
3	1.05	15.11	3.60	3.12	2.29	./.
4	0.89	56.96	11.61	8.13	2.42	./.
5	0.93	18.23	3.80	2.91	1.58	./.
6	1.29	11.87	2.79	2.59	1.09	./.
7	1.43	14.53	3.08	3.09	2.06	./.
8	1.49	16.85	3.37	3.23	1.64	./.
9	1.29	10.44	2.27	2.26	1.05	./.
10	1.39	18.87	4.07	4.13	1.67	./.
11	0.98	18.20	3.89	3.39	2.29	./.
12	0.89	15.00	3.18	3.01	1.39	./.
13	0.94	9.23	1.97	2.17	1.72	./.
14	1.24	7.93	1.66	1.93	1.43	./.
15	1.05	7.73	1.85	2.23	0.97	./.
16	0.63	8.37	1.88	2.16	1.58	./.
17	0.46	8.92	1.75	1.03	1.54	./.
18	0.24	3.00	0.77	1.26	0.72	./.
19	0.30	7.36	1.29	1.32	0.79	./.
20	1.14	24.49	5.72	4.02	2.23	./.
21	1.23	19.92	4.88	2.87	1.94	./.
22	0.76	17.48	4.16	2.94	1.93	./.
23	0.39	3.44	0.91	0.87	0.80	./.
24	0.81	13.75	3.10	2.33	1.13	./.
25	0.27	4.71	0.94	0.85	0.82	./.
26	0.80	11.66	2.63	1.81	1.33	./.
27	0.33	4.14	1.12	0.98	0.99	./.
28	0.61	6.70	1.84	1.63	1.66	./.
29	1.21	13.31	3.31	2.85	2.26	./.
30	1.09	10.99	2.62	2.61	2.32	./.
31	1.22	13.32	3.19	2.90	2.92	./.

Radioactivity pc/m^3

Apr 1976	fallout $.10^{-2}$	Be7 $.10^{-2}$	P32 $.10^{-3}$	P33 $.10^{-3}$	S35 $.10^{-3}$	O3 ppb
1	1.55	15.74	3.33	2.72	1.21	./.
2	1.95	17.53	3.63	2.98	1.16	./.
3	1.45	16.61	3.78	2.23	2.63	./.
4	1.36	9.81	2.37	1.62	2.29	./.
5	1.07	6.66	1.61	1.73	0.69	./.
6	1.08	8.84	1.84	1.59	0.58	./.
7	0.34	2.93	0.68	0.80	0.71	./.
8	0.24	2.13	0.59	0.81	0.82	./.
9	0.44	4.58	1.41	1.28	1.16	./.
10	0.54	8.46	7.35	5.16	2.72	./.
11	0.49	22.20	5.32	4.17	2.01	./.
12	1.55	16.42	4.36	2.47	1.61	./.
13	1.33	12.12	2.83	2.69	1.66	./.
14	1.28	9.15	2.34	2.14	1.29	./.
15	1.54	9.16	2.42	2.20	1.52	./.
16	1.42	11.34	2.72	2.81	1.70	./.
17	1.11	10.19	2.60	1.72	0.86	./.
18	1.35	13.26	3.29	2.02	1.40	./.
19	1.73	13.57	3.40	2.34	2.10	./.
20	1.76	12.32	3.08	2.03	1.25	./.
21	1.11	11.90	2.90	1.73	1.46	./.
22	0.77	6.92	1.79	1.25	0.92	./.
23	0.14	1.50	0.66	1.14	0.93	./.
24	0.22	1.71	0.32	0.66	0.78	./.
25	0.15	1.60	0.44	0.89	1.07	./.
26	0.27	1.60	0.88	0.76	0.80	./.
27	0.60	7.21	1.93	2.24	0.76	./.
28	0.94	25.35	5.76	5.25	0.81	./.
29	1.29	43.46	10.22	7.73	6.11	./.
30	1.09	16.77	4.03	3.92	2.14	./.

Radioactivity pc/m^3

Mai 1976	fallout $.10^{-2}$	Be7 $.10^{-2}$	P32 $.10^{-3}$	P33 $.10^{-3}$	S35 $.10^{-3}$	03 ppb
1	1.47	17.32	4.12	2.93	2.61	./.
2	1.54	20.38	4.35	3.48	3.25	./.
3	0.76	9.90	2.17	2.35	1.36	./.
4	0.40	4.50	1.18	1.01	0.44	./.
5	1.27	14.70	3.27	2.60	2.53	./.
6	1.78	18.02	3.66	4.20	3.73	./.
7	1.98	16.39	3.60	3.73	3.08	./.
8	1.87	15.56	3.76	3.30	2.91	./.
9	0.85	9.30	1.95	1.72	1.45	./.
10	0.61	7.80	1.74	2.12	1.81	./.
11	0.53	6.34	1.58	1.97	1.14	./.
12	0.62	5.30	1.31	1.64	0.91	./.
13	0.16	2.51	0.74	1.15	0.92	./.
14	0.84	25.87	6.18	4.36	2.86	./.
15	1.04	20.91	5.08	4.34	2.85	./.
16	1.52	15.79	3.65	3.75	2.81	./.
17	1.59	15.45	3.69	3.43	2.85	./.
18	1.59	18.24	4.30	3.91	2.64	./.
19	0.94	11.42	2.71	2.81	1.86	./.
20	0.37	2.54	0.77	0.84	0.81	./.
21	0.17	1.15	0.44	0.85	0.87	./.
22	0.43	7.20	1.52	1.49	1.24	./.
23	0.43	7.20	1.52	1.49	1.24	./.
24	0.77	21.37	4.62	4.38	2.44	./.
25	./.	./.	./.	./.	./.	./.
26	0.22	4.41	0.42	0.81	0.51	./.
27	0.44	1.91	1.25	1.30	0.92	./.
28	0.93	16.15	3.45	3.49	2.51	./.
29	1.30	16.18	3.31	3.05	2.14	./.
30	0.51	7.00	1.64	2.11	1.58	./.
31	0.20	2.85	0.80	1.10	0.57	./.

Radioactivity pc/m^3

Juni 1976	fallout $.10^{-2}$	Be7 $.10^{-2}$	P32 $.10^{-3}$	P33 $.10^{-3}$	S35 $.10^{-3}$	03 ppb
1	0.13	1.33	0.34	0.73	0.30	./.
2	0.18	0.82	0.25	0.58	0.41	./.
3	0.23	1.91	0.64	1.01	0.58	./.
4	0.27	3.69	0.88	1.15	0.68	./.
5	0.68	12.63	2.69	2.91	1.73	./.
6	0.99	25.54	5.65	4.81	2.05	./.
7	0.74	24.07	5.63	4.61	2.45	./.
8	1.00	18.59	3.96	3.37	2.02	./.
9	1.37	15.52	3.29	3.13	1.85	./.
10	1.00	14.88	3.34	3.29	2.17	./.
11	1.29	15.86	3.41	3.35	1.60	./.
12	1.15	13.85	3.18	2.72	1.86	./.
13	1.23	12.20	2.74	2.70	1.52	./.
14	1.05	11.81	2.77	2.67	1.61	./.
15	1.21	13.46	2.61	2.77	1.66	./.
16	0.48	9.03	1.75	2.45	1.87	./.
17	0.75	19.05	4.48	3.59	1.70	./.
18	1.02	18.76	3.91	3.63	2.66	./.
19	1.20	19.81	4.21	3.89	2.33	./.
20	1.31	13.71	2.65	3.21	1.63	./.
21	1.30	13.06	3.01	2.76	1.90	./.
22	1.49	13.24	2.73	2.91	1.57	./.
23	1.02	15.64	2.58	2.84	2.01	./.
24	1.03	12.94	3.59	3.06	2.27	./.
25	1.17	13.22	3.13	2.94	1.09	./.
26	1.00	19.94	4.36	3.83	2.96	./.
27	1.27	22.25	5.16	3.56	2.90	./.
28	0.88	20.97	4.57	3.72	2.70	./.
29	1.44	19.80	4.00	3.93	3.25	./.
30	1.32	14.38	3.12	3.22	1.53	./.

Radioactivity pc/m^3

Juli 1976	fallout $.10^{-2}$	Be7 $.10^{-2}$	P32 $.10^{-3}$	P33 $.10^{-3}$	S35 $.10^{-3}$	03 ppb
1	1.06	17.76	3.99	3.22	1.82	./.
2	1.35	19.49	3.95	3.71	2.45	./.
3	1.34	21.21	5.06	4.18	2.30	./.
4	1.49	23.41	5.80	3.94	3.25	./.
5	1.80	23.94	5.44	4.41	1.76	./.
6	1.79	21.97	4.46	3.63	1.33	./.
7	1.18	22.81	4.93	3.65	2.82	./.
8	1.30	18.22	4.33	3.99	4.05	./.
9	0.99	13.11	3.05	2.85	3.03	./.
10	0.29	7.33	1.22	1.56	2.17	./.
11	1.02	10.31	3.06	2.29	2.58	./.
12	1.05	10.02	2.47	2.18	3.12	./.
13	0.74	9.85	2.68	2.10	2.01	./.
14	./.	9.40	1.43	1.52	2.77	./.
15	1.02	14.55	3.49	3.19	2.92	./.
16	1.31	16.02	3.57	3.29	2.47	./.
17	1.28	13.00	2.85	4.90	2.73	./.
18	1.39	23.85	3.93	2.99	3.43	./.
19	0.86	20.43	3.45	2.85	1.83	./.
20	0.67	10.63	2.60	2.08	1.57	./.
21	0.43	8.94	2.24	2.36	1.20	./.
22	0.13	1.03	0.26	1.31	3.28	./.
23	0.24	0.91	0.21	0.86	3.25	./.
24	0.25	3.78	0.68	1.47	2.98	./.
25	0.15	0.69	0.20	0.79	2.02	./.
26	0.39	6.16	1.87	1.30	1.47	./.
27	0.32	5.05	1.41	1.17	1.28	./.
28	0.64	13.13	2.21	1.87	1.19	./.
29	0.90	24.93	4.77	2.80	2.06	./.
30	0.96	15.39	3.55	2.37	1.17	./.
31	0.55	6.60	1.64	1.42	0.68	./.

XIII

Radioactivity pc/m^3

Aug 1976	fallout $.10^{-2}$	Be7 $.10^{-2}$	P32 $.10^{-3}$	P33 $.10^{-3}$	S35 $.10^{-3}$	03 ppb
1	0.27	8.49	2.59	1.84	1.88	./.
2	0.49	13.47	3.49	2.92	1.87	./.
3	0.94	16.03	3.66	3.27	2.94	./.
4	0.53	9.47	2.35	1.94	1.50	./.
5	0.53	8.43	1.97	2.12	1.65	./.
6	0.53	9.32	2.32	2.25	0.57	./.
7	1.23	18.66	4.47	4.24	2.40	./.
8	1.43	17.75	4.21	3.66	3.23	./.
9	0.94	15.04	3.56	3.23	2.39	./.
10	0.40	4.91	1.16	1.04	0.88	./.
11	0.61	6.26	1.77	1.43	4.42	./.
12	1.06	12.04	2.18	2.42	1.98	./.
13	1.13	13.88	3.49	2.50	2.03	./.
14	1.29	14.37	3.58	3.36	2.10	./.
15	1.37	17.44	4.94	3.32	2.78	./.
16	1.22	14.09	3.85	4.12	2.34	./.
17	0.66	8.59	2.14	1.95	1.55	./.
18	0.80	10.04	2.38	1.92	1.38	./.
19	0.98	9.73	2.66	2.65	2.65	./.
20	0.78	8.04	2.21	2.25	2.27	./.
21	0.82	17.93	4.36	3.91	2.87	./.
22	1.38	20.89	5.32	4.47	3.54	./.
23	1.07	14.80	3.72	3.02	1.92	./.
24	1.67	18.14	5.07	4.40	3.29	./.
25	1.70	23.20	6.09	3.56	4.22	./.
26	1.72	19.67	4.99	3.00	1.79	./.
27	1.22	13.96	2.92	1.42	1.41	./.
28	0.93	10.31	2.60	1.52	0.95	./.
29	0.92	8.45	2.13	0.90	0.70	./.
30	0.41	7.23	1.62	0.88	0.84	./.
31	0.29	4.80	1.06	0.79	0.82	./.

Radioactivity pc/m^3

Sep 1976	fallout $.10^{-2}$	Be7 $.10^{-2}$	P32 $.10^{-3}$	P33 $.10^{-3}$	S35 $.10^{-3}$	03 ppb
1	0.39	3.43	0.78	0.58	0.60	./.
2	0.75	6.60	1.56	1.31	1.70	./.
3	0.16	1.89	0.50	0.58	0.32	./.
4	0.09	1.13	0.26	0.30	0.60	./.
5	0.33	2.39	0.58	0.48	0.21	./.
6	1.08	21.66	7.30	3.15	1.95	./.
7	1.03	24.25	7.34	3.29	1.19	./.
8	0.93	19.83	4.70	4.41	1.45	./.
9	1.13	10.74	2.68	2.27	0.67	./.
10	0.28	7.63	2.05	0.66	1.11	./.
11	0.72	22.49	5.69	4.12	2.10	./.
12	0.59	8.37	1.94	0.94	0.78	./.
13	0.18	1.77	0.71	0.90	0.84	./.
14	0.43	11.55	2.63	1.41	1.29	./.
15	0.29	4.52	1.12	0.83	0.47	./.
16	0.14	2.30	0.31	0.43	0.39	./.
17	0.43	2.95	0.73	0.61	0.92	./.
18	0.55	6.01	1.34	0.57	1.37	./.
19	1.66	16.87	3.34	2.34	1.47	./.
20	1.15	11.65	3.07	2.07	1.34	./.
21	2.22	20.05	4.39	3.10	1.27	./.
22	1.36	15.97	3.71	2.38	1.18	./.
23	1.19	16.39	3.47	2.50	1.52	./.
24	1.83	14.92	3.26	1.79	1.44	./.
25	1.89	14.50	4.32	3.38	2.63	./.
26	1.43	12.91	3.76	2.75	2.24	./.
27	0.96	9.30	3.28	2.16	1.36	./.
28	1.05	7.45	2.49	1.58	1.57	./.
29	0.20	4.52	2.07	0.93	1.06	./.
30	0.46	6.56	1.60	1.78	1.12	./.